

AD-A052 610

CALIFORNIA RESEARCH AND TECHNOLOGY INC WOODLAND HILLS

F/G 13/13

INTERACTIONS OF STRESS WAVES WITH DEEPLY-BURIED TUNNELS IN GEOL--ETC(U)

JAN 76 M ROSENBLATT, G E EGGUM, Y M ITO

DNA001-74-C-0176

UNCLASSIFIED

CRT-2040-2

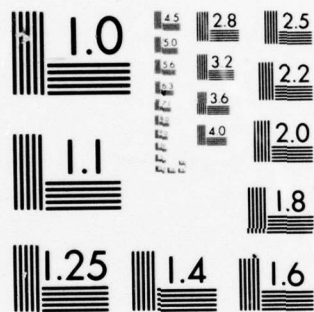
DNA-4398F

NL

| OF |

AD  
A052610





MICROCOPY RESOLUTION TEST CHART  
NATIONAL BUREAU OF STANDARDS-1963-A

3-27-78

AD-E 300 140

DNA 4398F

AD A052610

# INTERACTIONS OF STRESS WAVES WITH DEEPLY-BURIED TUNNELS IN GEOLOGIES WITH CRACKS AND DISCONTINUITIES

12  
at

California Research & Technology, Inc.  
6269 Variel Avenue  
Woodland Hills, California 91367

JANUARY 1976

Final Report for Period February 1974—January 1976

CONTRACT No. DNA 001-74-C-0176

APPROVED FOR PUBLIC RELEASE;  
DISTRIBUTION UNLIMITED.

THIS WORK SPONSORED BY THE DEFENSE NUCLEAR AGENCY  
UNDER RDT&E RMSS CODE B344075462 J34EAXSX31101 H2590D.

Prepared for  
Director  
DEFENSE NUCLEAR AGENCY  
Washington, D. C. 20305

DDC  
RECEIVED  
APR 13 1978  
B

AD No.   
DDC FILE COPY

(18) DNA, SBIE

UNCLASSIFIED

SECURITY CLASSIFICATION OF THIS PAGE (When Data Entered)

19 REPORT DOCUMENTATION PAGE		READ INSTRUCTIONS BEFORE COMPLETING FORM	
1. REPORT NUMBER DNA 4398F, AD-E392124	2. GOVT ACCESSION NO.	3. RECIPIENT'S CATALOG NUMBER	
4. TITLE (and Subtitle) INTERACTIONS OF STRESS WAVES WITH DEEPLY-BURIED TUNNELS IN GEOLOGIES WITH CRACKS AND DISCONTINUITIES.	5. TYPE OF REPORT AND PERIOD COVERED Final Report, for Period February 1974-January 1976	6. PERFORMING ORG. REPORT NUMBER CRT-2040-2	
7. AUTHOR(s) M. Rosenblatt, Y. M. Ito G. E. Eggum, K. N. Kreyenhagen	8. CONTRACT OR GRANT NUMBER(s) DNA 001-74-C-0176 new	9. PERFORMING ORGANIZATION NAME AND ADDRESS California Research & Technology, Inc. 6269 Variel Avenue Woodland Hills, California 91367	10. PROGRAM ELEMENT, PROJECT, TASK AREA & WORK UNIT NUMBERS NWET Subtask J34EAXS311-01 17X312
11. CONTROLLING OFFICE NAME AND ADDRESS Director Defense Nuclear Agency Washington, D.C. 20305	12. REPORT DATE JAN 76	13. NUMBER OF PAGES 72	14. MONITORING AGENCY NAME & ADDRESS (if different from Controlling Office) 1268p.
15. SECURITY CLASS (of this report) UNCLASSIFIED		15a. DECLASSIFICATION/DOWNGRADING SCHEDULE	
16. DISTRIBUTION STATEMENT (of this Report) Approved for public release; distribution unlimited.			
17. DISTRIBUTION STATEMENT (of the abstract entered in Block 20, if different from Report)			
18. SUPPLEMENTARY NOTES This work sponsored by the Defense Nuclear Agency under RDT&E RMSS Code B344075462 J34EAXSX31101 H2590D.			
19. KEY WORDS (Continue on reverse side if necessary and identify by block number) Block Motion      Deeply Buried Structures Joints              Coupled Finite Difference-Finite Element Code			
20. ABSTRACT (Continue on reverse side if necessary and identify by block number) The purpose of this study was to examine the response of deeply-buried tunnels to the effects of high stress dynamic loading. In the Phase I portion of the study, attention was concentrated on the effects of geologic discontinuities (e.g., joints) on tunnels, with particular emphasis on the interactions between joints and backpacking. In Phase II, emphasis was on the response of integral tunnels in hard and soft rock geologies, and on the implementation of a coupled finite element/finite difference method (called			

DD FORM 1 JAN 73 1473 EDITION OF 1 NOV 65 IS OBSOLETE

UNCLASSIFIED

SECURITY CLASSIFICATION OF THIS PAGE (When Data Entered)

391 223

LB



UNCLASSIFIED

SECURITY CLASSIFICATION OF THIS PAGE(When Data Entered)

20. ABSTRACT (Continued)

LAP, for Linked Analysis Program) for analyzing the response of thin liners to dynamic loading in geologic media.

In this report, a summary is provided of the Phase I work, and a more detailed discussion is given of the Phase II effort. Recommendations are made as to work which might be conducted in an on-going program.

UNCLASSIFIED

SECURITY CLASSIFICATION OF THIS PAGE(When Data Entered)

## TABLE OF CONTENTS

1.	INTRODUCTION AND SUMMARY OF RESULTS OF PHASE I . . . . .	3
2.	SUMMARY OF RESULTS OF PHASE II, AND RECOMMENDATIONS FOR CONTINUING EFFORT . . . . .	10
2.1	Phase II Summary . . . . .	10
2.2	Recommendations. . . . .	12
3.	MATERIAL PROPERTIES FOR NUMERICAL SOLUTIONS . . . . .	15
3.1	Tuff . . . . .	15
3.1.1	Equation of State . . . . .	15
3.1.2	Failure . . . . .	16
3.2	Granite. . . . .	19
3.3	Concrete . . . . .	19
4.	UNLINED AND CONCRETE-LINED TUNNELS. . . . .	21
4.1	Unlined Tunnel in Granite. . . . .	21
4.2	Concrete Liners in Tuff - Comparisons Showing Effects of Different Failure Models. . . . .	26
4.3	Unlined vs Concrete-Lined Tunnels in Tuff. . . . .	31
5.	COUPLED FINITE DIFFERENCE/FINITE ELEMENT LAP CODE FOR ANALYSIS OF THIN LINERS. . . . .	37
6.	DEFORMABLE STEEL LINERS . . . . .	39
6.1	Two-Inch Steel Liner in Tuff (Case M). . . . .	39
6.2	Two-Inch Steel Liner Backed by Two Feet of Concrete in Tuff (Case N) . . . . .	40
	REFERENCES. . . . .	42

ACCESSION for		
NTIS	White Section	<input checked="" type="checkbox"/>
DDC	Buff Section	<input type="checkbox"/>
UNANNOUNCED		<input type="checkbox"/>
JUSTIFICATION _____		
BY _____		
DISTRIBUTION/AVAILABILITY CODES		
Dist.	AVAIL.	and/or SPECIAL
<b>A</b>		

## 1. INTRODUCTION AND SUMMARY OF RESULTS OF PHASE I

All rock masses contain large numbers of nominally planar discontinuities, such as joints, faults, cracks, and bedding planes. These surfaces usually have properties which are quite different from the basic medium, and there is both experimental<sup>1</sup> and theoretical<sup>2</sup> evidence to suggest that the effects of these discontinuities should be one of the important considerations involved in designing survivable underground structures.

In extreme cases, the sliding of material along joints or other discontinuities could cut off a buried structure (by guillotining), or it could split a tunnel lengthwise, as shown in the sketches below. In less extreme cases, the situation shown in Figure 1 may develop, where portions of the tunnel wall attempt to project into the tunnel. The tunnel liner must resist such motion. Backpacking, of course, makes it easier for a tunnel liner to accommodate small displacements without damage.



In the Phase I study, interactions of the type shown in Figure 1 between deeply-buried tunnels and *in situ* joints in granite when loaded by 1 kb stress waves were investigated using both analytical models and two-dimensional finite

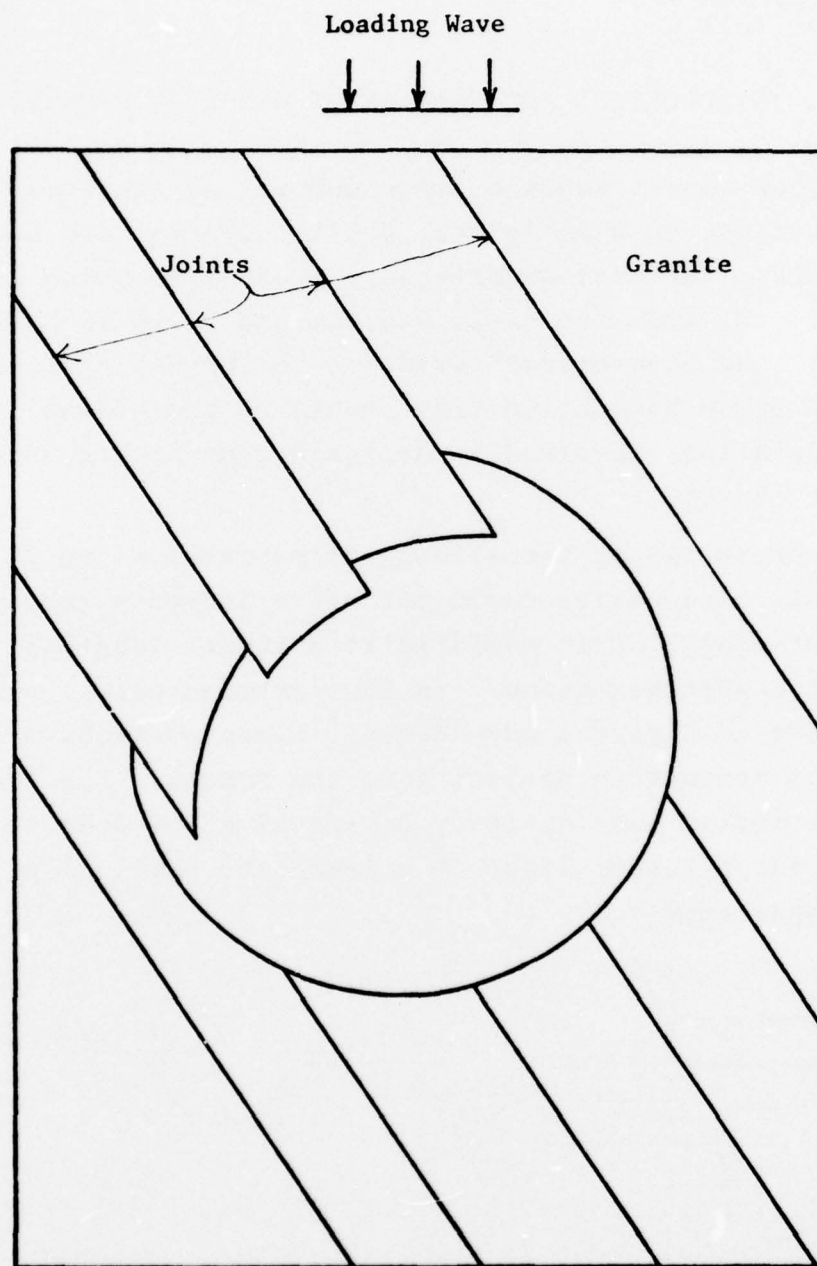


Figure 1. Damage Mode from Local Block Motions Near Tunnels Considered in Phase I of Study



difference numerical code calculations. The study consisted of (1) the development and use of analytical solutions to simplified models to predict if, and where slippage of joints occurs near a tunnel, (2) the development of a model which provides a conservative estimate of the ability of a backpacking system to resist and accommodate block motions, and (3) the generation of seven exploratory numerical solutions (using the Lagrangian WAVE-L finite difference code) to examine the time-resolved wave propagation interactions between various lined and unlined tunnels, with and without joints present in the surrounding rock. The conditions for these numerical solutions in Phase I are listed in Table 1. All of the solutions were two-dimensional, plane strain cases treating a 1 kb planar step wave incident on an infinite cylindrical tunnel. Models were developed for use in the numerical solutions to describe the hydrodynamic, elastic, and failure properties of the backpacking material. Also, constitutive properties were formulated for dilatant rock joints.

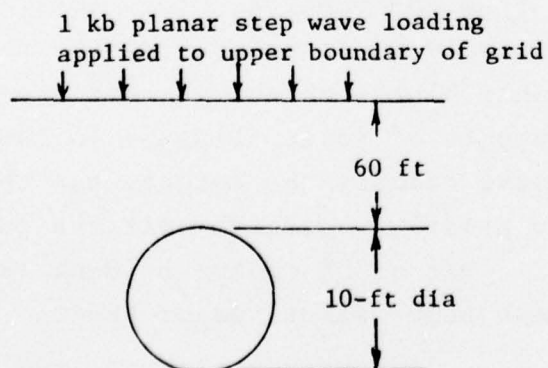
Two important, related conclusions can be drawn from the results of the Phase I study:

1. Significant block motions and joint slippage in the immediate vicinity of a tunnel will be primarily activated by stress relief waves emanating from the opening. This activation of joint motions is most likely to occur near the tunnel springlines, but it involves only blocks which are near the tunnel. There may be small amounts of joint slippage in the free field before the stress wave reaches the tunnel, but the tendency for joint slippage is greatly increased near the tunnel due to local stress relief. (It is of course evident that large relative displacements can occur across major fault



Table 1. Conditions for Numerical Solutions  
in Phase I Portion of Study

<u>Case</u>	<u>Medium</u>	<u>Joints</u>	<u>Backpacking</u>	<u>Liner</u>
A	Granite	None	None	Unlined
B	Granite	~3' spacing, frictionless, ⊥ to wave front	None	Unlined
C	Granite	None	5' simulated backpacking	1" rigid steel
D	Granite w/no tensile failure	3' spacing, diag. to wave, dilatent w/friction	None	Unlined
E	Granite	3' spacing, diag. to wave, dilatent w/friction	None	Unlined
F	Granite	3' spacing, diag. to wave, dilatent w/friction	None	1" rigid steel
G	Granite	3' spacing, diag. to wave, dilatent w/friction	5' cellular concrete, $P_c = 1500$ psi	3/8" rigid steel



1' nominal zoning  
used in all problems.  
Tunnels were at 4000'  
depth.

planes or long planar surfaces with low shear resistance, with or without the presence of a tunnel, but we were not concerned with these large-scale phenomena in this study.)

2. Backpacking and friction are very effective in limiting these local block motions for 0.5 - 1.5 kb stress loads on deeply-buried tunnels. Figures 2 and 3 show estimates (obtained from an analytical model) of the thicknesses of backpacking required to stop a block of length  $L$  which has been accelerated into a tunnel by 0.5, 1.0, and 1.5 kb stress loads. The backpacking resists the block penetration with a crushing stress of 1900 psi in uniaxial strain. After the backpacking has sustained 9% strain, it begins to lock up, and stresses rise sharply above 1900 psi. In our conservative model, we assumed that this condition would result in tunnel failure. Figure 2 shows the extreme case of frictionless, or open joints. Even in this worst case, 11 inches of backpacking is sufficient to stop a 10-ft long block accelerated by a 1 kb wave. 25 inches of backpacking are required for a 1.5 kb wave. Figure 3 illustrates the effectiveness of frictional forces acting along the joints bounding the moving block. With a nominal frictional shear stress of 100 bars (which roughly corresponds to a "wet" joint), only 4.5 in. and 10 in., respectively, are required to stop a 10-ft long block accelerated by 1 kb and 1.5 kb waves.

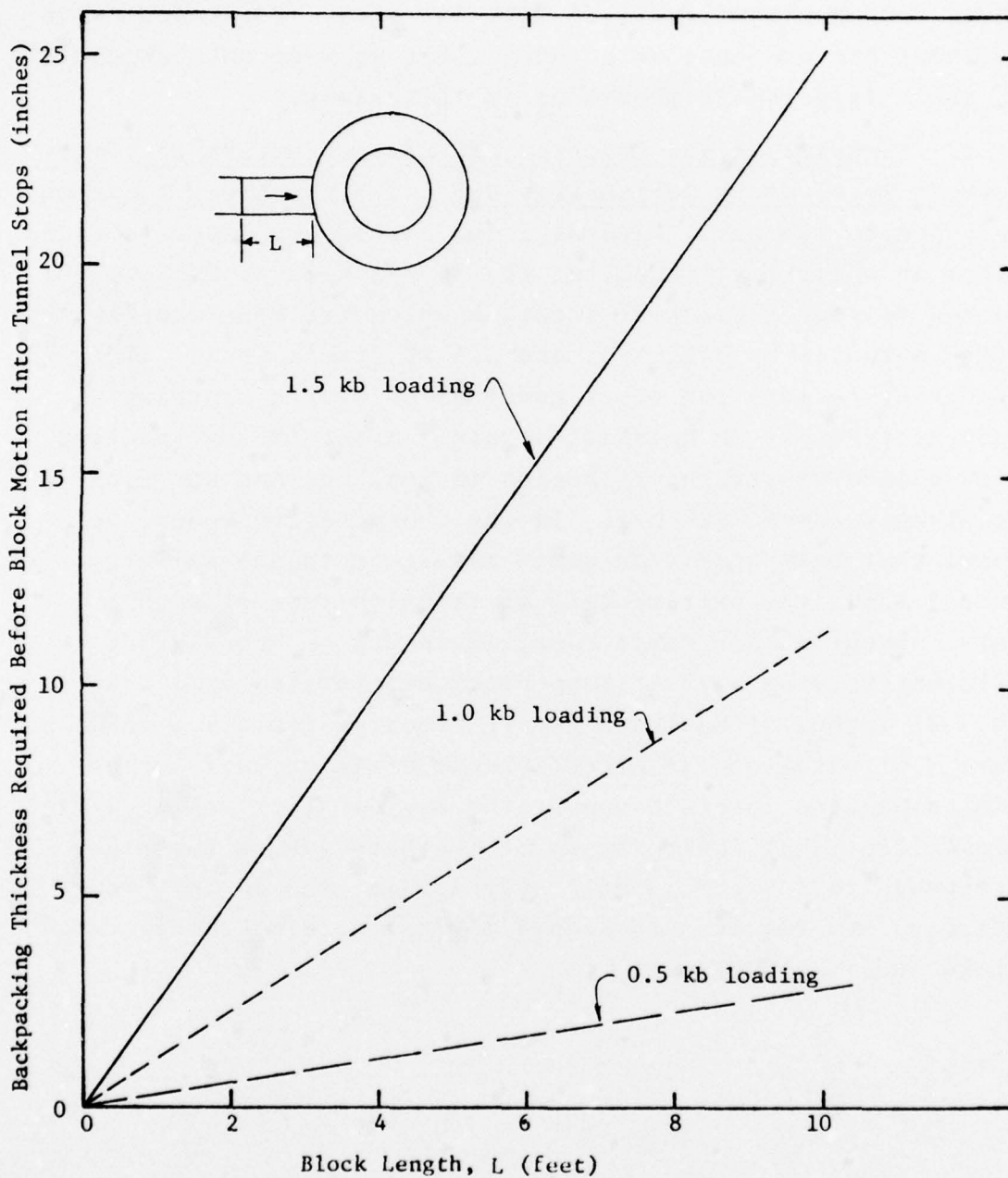


Figure 2. Backpacking Thickness Required to Stop a Block Accelerated into a Tunnel by Stress Loadings of 0.5, 1.0, and 1.5 kb (No friction)

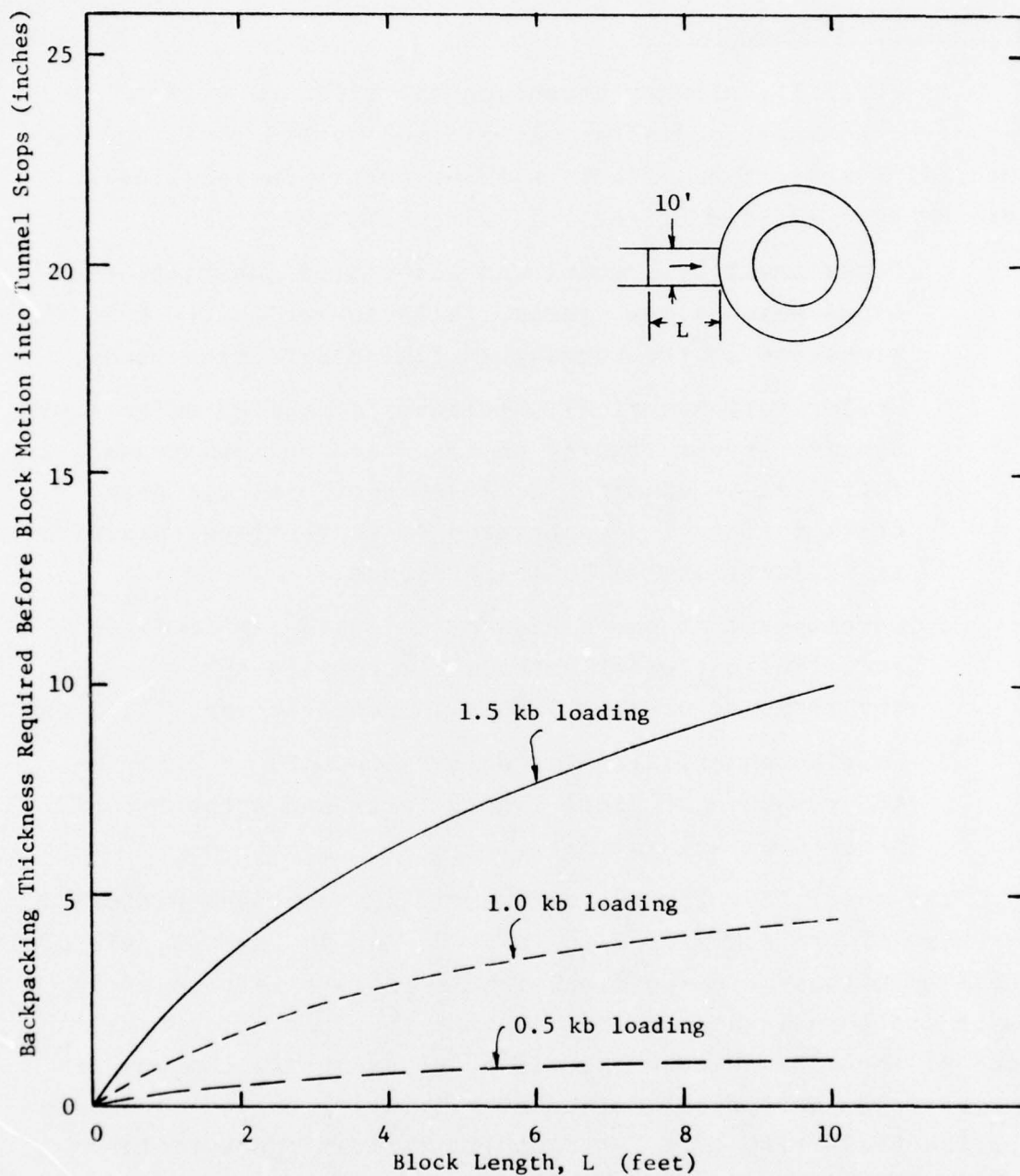


Figure 3. Backpacking Thickness Required to Stop a Block Accelerated into a Tunnel by Stress Loadings of 0.5, 1.0, and 1.5 kb (100 bar frictional stress on sliding surfaces of block)



## 2. SUMMARY OF RESULTS OF PHASE II, AND RECOMMENDATIONS FOR CONTINUING EFFORT

### 2.1 PHASE II SUMMARY

In Phase II, primary attention was given to liners in softer geologic media, as exemplified by NTS tuff, and to integral liners (i.e., liners without porous backpacking).

This Phase consisted of the following main efforts:

- o Development of a model and associated numerical technique which allow shear cracks to explicitly form and propagate in the Lagrangian finite difference code,
- o Exploratory numerical solutions to examine effects of dynamic stress loading on lined and unlined tunnels in tuff, and to examine the effects of explicit shear crack failure (as contrasted to conventional plasticity failure) on the tunnel response,
- o Development of the LAP code, a linked finite difference/finite element method, for coupled analysis of the response of thin liners in geologic materials, and
- o Coupled numerical solutions, using LAP, to analyze the response of steel liners (with and without concrete backing) in tuff.

The conditions for the six numerical solutions performed in Phase II are summarized in Table 2. As in Phase I, all of these solutions were two-dimensional, plane strain cases in which the tunnel was subjected to a 1 kb planar step wave. Some of these cases were exercising or demonstrating new aspects of the analytical methods for treating buried structures for the first time (i.e., the explicit shear crack failure model and the coupled LAP code).

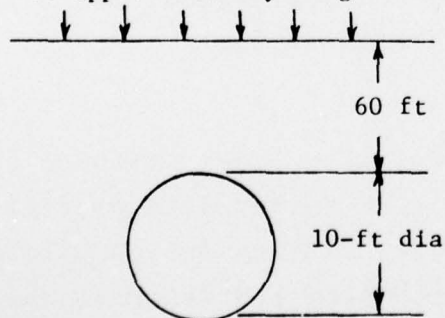
The results of the Phase II efforts are described in the balance of this report. The most important of the



Table 2. Conditions for Numerical Solutions  
in Current Phase II Portion of Study

<u>Case</u>	<u>Medium</u>	<u>Fracture Model</u>	<u>Liner:</u>		<u>Remarks</u>
			<u>Thickness</u>	<u>Material</u>	
H	Granite	Explicit shear cracks	Unlined		
J	NTS Tuff	Plasticity	Unlined		
K	NTS Tuff	Plasticity	1-ft	Concrete	
L	NTS Tuff	Explicit shear cracks	1-ft	Concrete	
M	NTS Tuff	Explicit shear cracks	2-in	Deformable steel	LAP code (linked FE/
N	NTS Tuff	Explicit shear cracks	2-in	Deformable steel	FD) sol'ns
			+ 2-ft	Concrete	

1 kb planar step wave loading applied  
to upper boundary of grid



1' nominal zoning  
used in all problems.

findings are the following:

1. Shear cracks (and presumably tensile cracks also) which form near the tunnel as a consequence of the dynamic loading can lead to non-uniformities in velocities near lined tunnels, and hence to stress concentrations in liners. These stress concentrations will need to be taken into consideration in the design of integral liners.

2. The LAP code provides a practical method for analyzing the coupled dynamic response of thin liners and the surrounding medium. The finite difference portion of the method is used to analyze free field motions and the medium response (including joint slippage and generation of explicit cracks), while the finite element portion is used to analyze the response of the liner. This combination avoids the necessity of using small cells (and small time steps) to resolve action in a relatively thin liner in a purely finite difference analysis.

3. Two-inch steel liners in 10-ft dia tunnels in tuff subjected to 1 kb stress wave loading will experience stresses which are large enough to cause inelastic deformation. Diame-tral strains of about 2-3 inches develop shortly after the tunnel liner is engulfed by a 1 kb step wave. Accelerations (relative to the center of mass of the tunnel) associated with these distortions are of the order of 1000-3000 g's.

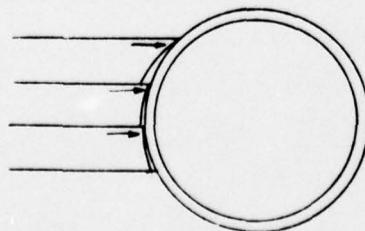
## 2.2 RECOMMENDATIONS

Using the coupled LAP method, realistic liner systems, as well as new liner concepts, should now be analyzed to predict their response in various media and with various design parameters. LAP is able to treat fairly complex 2-D designs, and to generate dynamic response predictions which would be very

useful in making preliminary evaluations of new concepts, in examining dynamic failure mechanisms, and in helping to optimize design variables. The following specific work is recommended:

1. New design concepts - The experimental evaluation of new design concepts is both expensive and time consuming. Small-scale experiments are useful for preliminary evaluations, but there are uncertainties and limitations in these tests relative to boundary conditions, material property simulation, and in observing potentially important dynamic phenomena on such small scale. LAP code solutions offer an alternative or supplementary approach for preliminary evaluations. Such solutions are particularly valuable in that they indicate the failure modes or weaknesses of new designs, thereby suggesting avenues for improvements.

2. Dynamic failure mechanisms - The Phase I results indicate that relative displacements across joints will not usually be larger than a few inches under conditions of interest. (We refer here to the local motions which are discussed in the Phase I summary in Section 1 above.) Such motions can be accommodated by backpacking, but they become a much more serious concern with integral liners, which must resist any motion which would lead to significant relative displacements near the tunnel. In resisting such motions, large local concentrations of forces applied to the liner may develop, as indicated in the sketch below:



In addition to force concentrations due to motions along preexisting joints or cracks, the work in Phase II with explicit crack propagation suggests that cracking which is induced by the stress wave loading near the tunnel may also produce non-uniformities in loading on the liner. The dynamics of such force concentrations and/or non-uniformities need to be considered in liner design.

We had hoped, during Phase II, to be able to analyze one or more cases such as shown by the sketch on the preceding page. However, we did not get that far after completion of the LAP code implementation. In addition, we felt that such analyses should be performed after we could treat both explicit shear cracking and tensile cracking simultaneously in the Lagrangian code. We recommend that this additional modeling capability be added now, and that the local interactions of displacement discontinuities with tunnel liners then be analyzed to determine the stress concentrations in liners.

3. Parameter optimization - The LAP method offers a fairly efficient way to conduct series of analyses which can be used to guide the optimization of design variables so as to obtain the maximum useable tunnel volume for a given excavated volume. Survivability criteria can be specified, for example, in terms of liner fracture, or maximum allowable distortion, velocity, or acceleration. Solutions of this type can be obtained at modest cost, and the results used to construct curves showing sensitivity of liner response to the design variable, medium properties, etc.



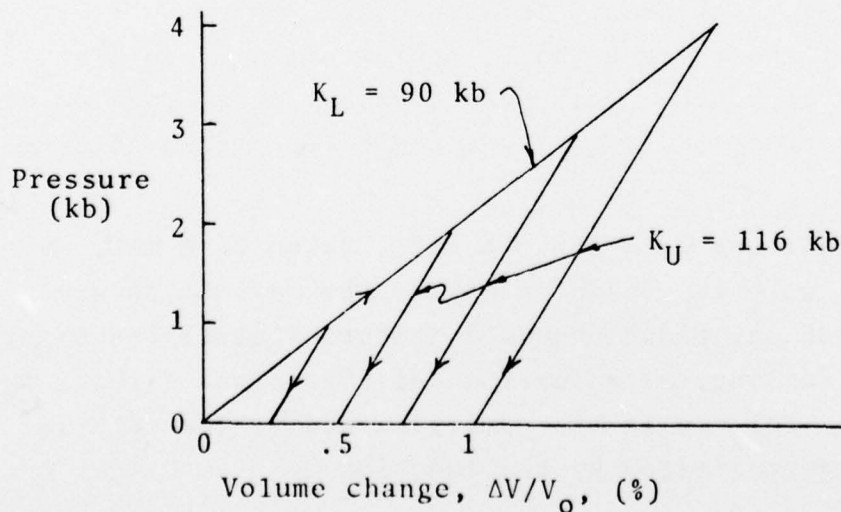
### 3. MATERIAL PROPERTIES FOR NUMERICAL SOLUTIONS

#### 3.1 TUFF

##### 3.1.1 Equation of State

Emphasis in the Phase II portion of this study has been on tunnels in relatively soft geologic materials. NTS tuff was chosen as being representative of these softer materials. Fairly extensive constitutive property data are available for this material, as summarized in Ref. 3. These data show that the properties of NTS tuff vary considerably with depth, water content, etc. Because of this variability, and because the peak overpressures experienced by the tuff in our solutions would be only about 1 kb, a relatively simple, hydrostatic equation of state with constant, but different, loading and unloading moduli was adopted, based on the data in Ref. 3. We believe the important characteristics of deeply-buried tuff in the stress range of concern here are adequately represented by this approach.

A sketch of the behavior of the hydrostatic equation of state used in loading and unloading is shown below:





As indicated, the tuff loads with a bulk modulus,  $K_L = 90$  kb. It unloads (and reloads) with a bulk modulus,  $K_U = 116$  kb. This behavior was chosen to model hysteretic compaction of the material. Unloading from 4 kb, for example, results in a volume reduction of 1%, which is consistent with experimental hydrostatic loading curves and residual volume compaction data for several NTS tuffs.

A constant shear modulus during loading and unloading was used, based on experimental bulk modulus and longitudinal sound speed data from Ref. 3. The values used were 28 kb for the shear modulus and  $C_D = 8500$  fps.

### 3.1.2 Failure

The failure properties of the tuff were modeled in two ways: The first, which we refer to as the plasticity model, is the conventional method in which failure is assumed to manifest itself as a yielding phenomenon occurring on a plastic yield surface. The rationale for this model is that the material fails by developing numerous small cracks which simulate plastic behavior. The second failure model, which we refer to as the explicit shear crack model, represents a refinement of the plasticity approach. This method allows the formation of explicit shear cracks, along with appropriate stress adjustments.

Material failure data for NTS tuff, taken from Ref. 4, are shown in Figure 4. These data give the maximum shear stress,  $\tau$ , which any plane embedded in the material can experience without failing, as a function of the normal stress,  $\sigma_n$ , on that plane. For use in the numerical model, the data in Figure 4 were approximated by the function

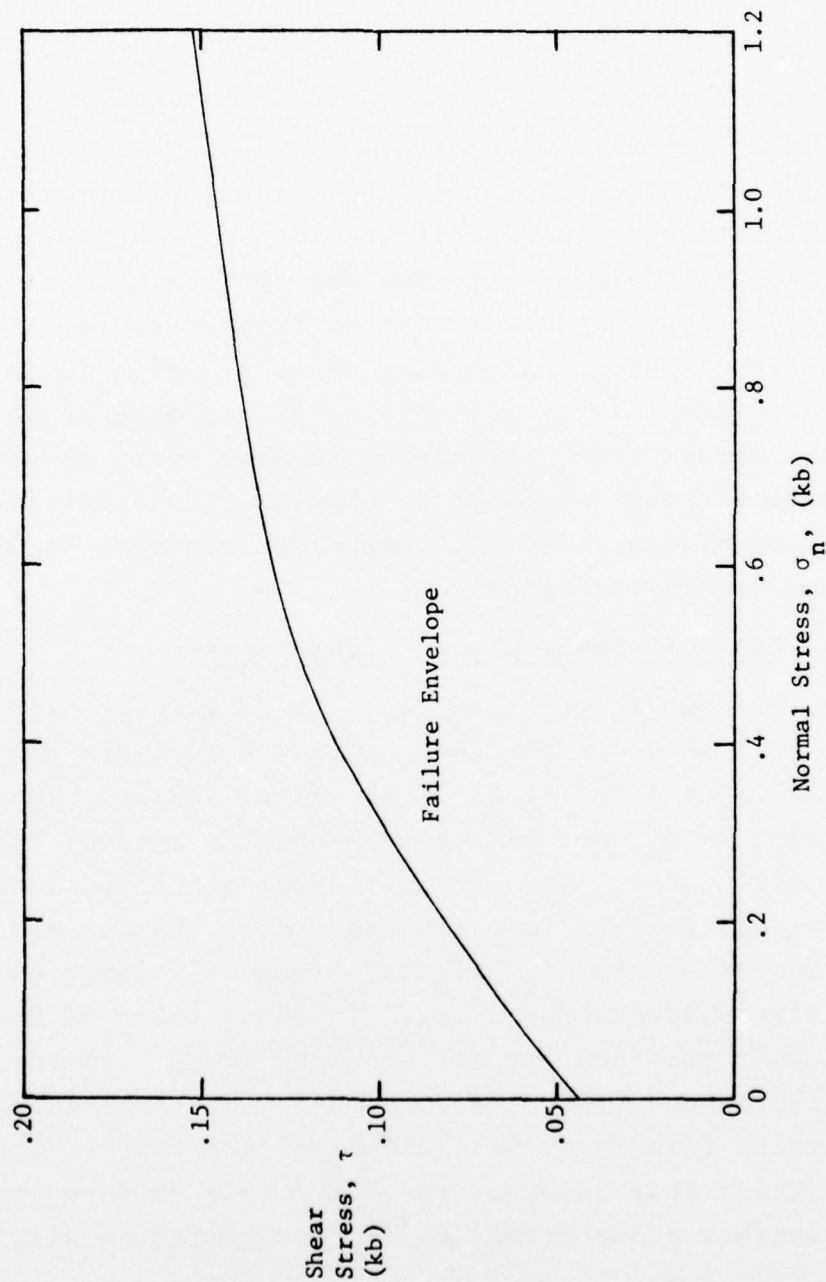


Figure 4. Maximum Shear Stress Which Can Be Withstood Across a Plane vs Normal Stress on Plane, NST Tuff (from Ref. 4)

$$\tau = \tau_{\infty} - c e^{\sigma_n / \sigma_0} \quad (1)$$

where

$$\begin{aligned} \tau_{\infty} &= .16 \text{ kb} \\ c &= .115 \text{ kb} \\ \sigma_0 &= .465 \text{ kb} \end{aligned}$$

a. Plasticity Failure Model

The yield stress for the conventional plasticity failure model was obtained from eq. (1) by interpreting the normal stress,  $\sigma_n$ , as the pressure, and the shear stress as being proportional to the yield stress at that pressure. The proportionality constant was chosen to be 2, which (under conditions of uniaxial strain) results in yielding being initiated at the stress level where shear cracks first appear. Since the numerical solutions have a uniaxial strain far field boundary condition, a direct comparison can thus be made between the two failure models.

b. Explicit Shear Crack Failure Model

In this model, material fails by developing explicit shear cracks whenever the shear stress across any plane exceeds the value given by eq. (1). After failure, appropriate stress adjustments are made in the cell to reflect the existence of the cracks. The explicit shear crack model also requires a post-failure function expressing the maximum shear stress across an already existing crack as a function of the normal stress across the crack. In the absence of better data, we used half the shear stress provided by eq. (1) for this post-failure condition. Note that in isotropic materials, shear cracks form in pairs: when the shear stress across one plane exceeds that required for a fracture to form, there is always another plane across which this criterion will also be

satisfied. Thus, in the code solutions, no cell ever develops a single shear crack; they always come in pairs. In field plots obtained from the numerical solutions, the orientation of the shear cracks is indicated by line segments which are drawn in each failed cell. If *more than two* shear cracks are formed in any cell, the plasticity failure model is thereafter adopted for the material in that cell.

Explicit tensile cracking has also been programmed in the WAVE-L Lagrangian code in connection with another application, but the combination of explicit tensile and shear cracking is not currently allowed in the code.

### 3.2 GRANITE

For the one granite solution in Phase II (Case H), a linear elastic material model with bulk modulus,  $K = 512 \text{ kb}$ , shear modulus,  $G = 293 \text{ kb}$ , and density,  $\rho = 2.7 \text{ g/cm}^3$  was assumed. The shear failure surfaces for wet and dry granite joints, as determined in the Phase I effort, are reproduced in Figure 5. For Case H, we assumed that the shear failure surface for intact granite is the same as for a dry granite joint.

### 3.3 CONCRETE

A simple, linear elastic equation of state was used to represent the concrete liners, with a bulk modulus,  $K = 270 \text{ kb}$ , and a shear modulus,  $G = 138 \text{ kb}$ . The concrete was not allowed to fail in these solutions.



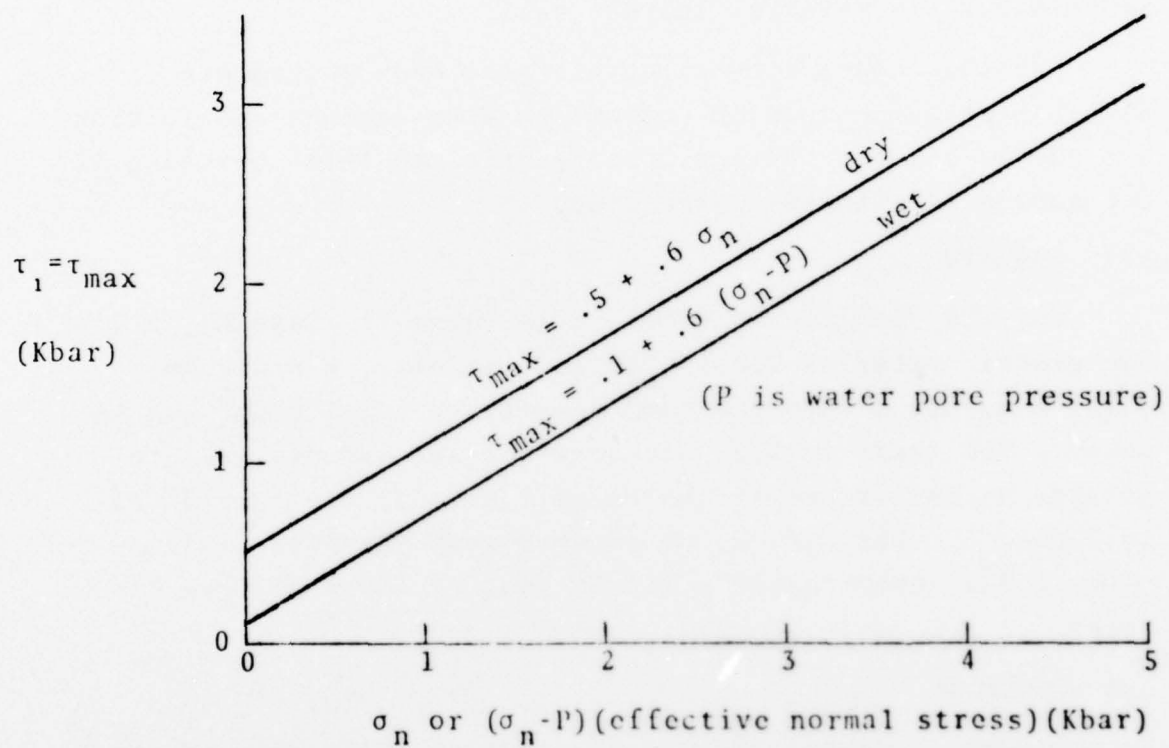


Figure 5. Shear Failure Surfaces for Wet and Dry Joints in Granite



#### 4. UNLINED AND CONCRETE-LINED TUNNELS

##### 4.1 UNLINED TUNNEL IN GRANITE

Case H involved an unlined tunnel in granite. The granite was modeled as being linear elastic, failing only when shear cracks develop. Tensile failure was not allowed. This was a preliminary solution, intended primarily to exercise the explicit shear crack model for the first time. The results have some interest as a comparison for later cases. In addition, the problem parameters are similar to those in the small-scale experiments being conducted at Stanford Research Institute<sup>5</sup>. Hence it offers some degree of code verification.

The two most prominent phenomena which are observed in the SRI experiments are (1) "flaking" at the springlines, and (2) long vertical cracks emanating from the springline region, as sketched in Figure 6.

Case H was run to 5.24 msec, which is about 2 msec after the stress wave strikes the top of the tunnel. Figures 7, 8, and 9 show the final grid configuration, velocity field, and principal stress field. Failed cells are denoted in the grid by line segments (aligned with the directions of the shear cracks) at the cell centers. Extensive shear fracture has occurred at the springlines in Figure 7, and flaking of the tunnel wall would result if the solution were continued. This tendency is seen in the effects of the stress relief afforded by the shear cracking in the velocity field (Figure 8). At 5.24 msec, however, the *shear* cracking is not propagating out of the springline region to form the long vertical cracks seen in the SRI experiments (as sketched in Figure 6). Rather, the stress plot in Figure 9 shows that significant *tensile* stresses

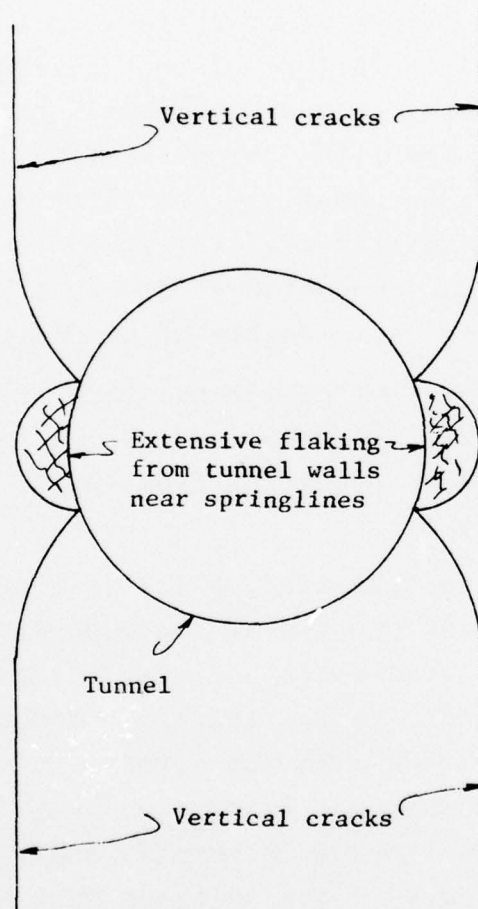


Figure 6. Sketch of Predominant Fracture Patterns Seen in SRI Small-Scale Tests

28 APR 75 CALIFORNIA RESEARCH AND TECHNOLOGY WAVE-L CODE  
CASE 2040-7 TUNNEL IN GRANITE, SHEAR CRACKS, NO BACKPACKING  
CYCLE 278

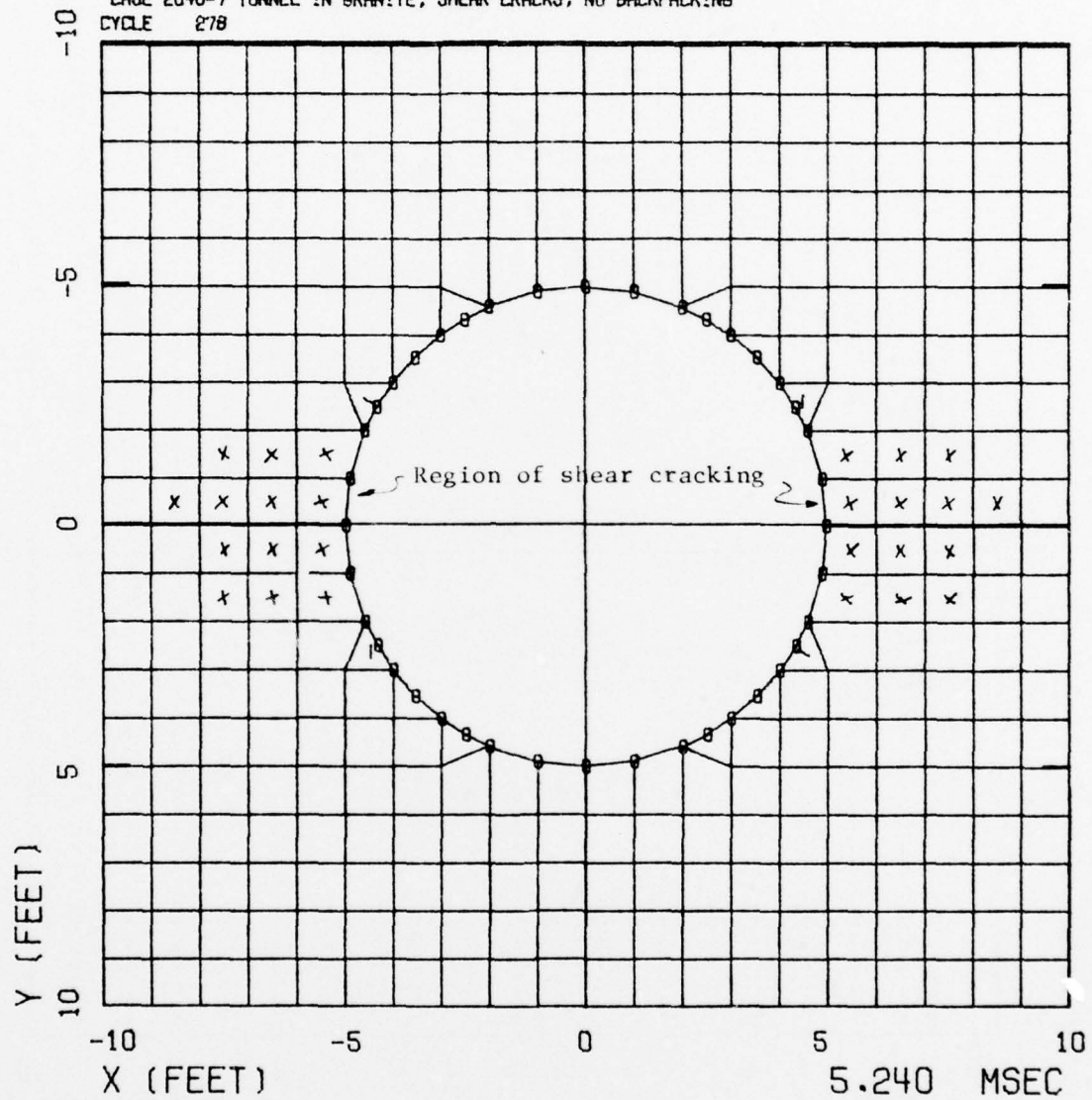


Figure 7. Case H - Unlined Tunnel in Granite with Explicit Shear Crack Failure Model. Final Grid Configuration (at 5.2 msec)

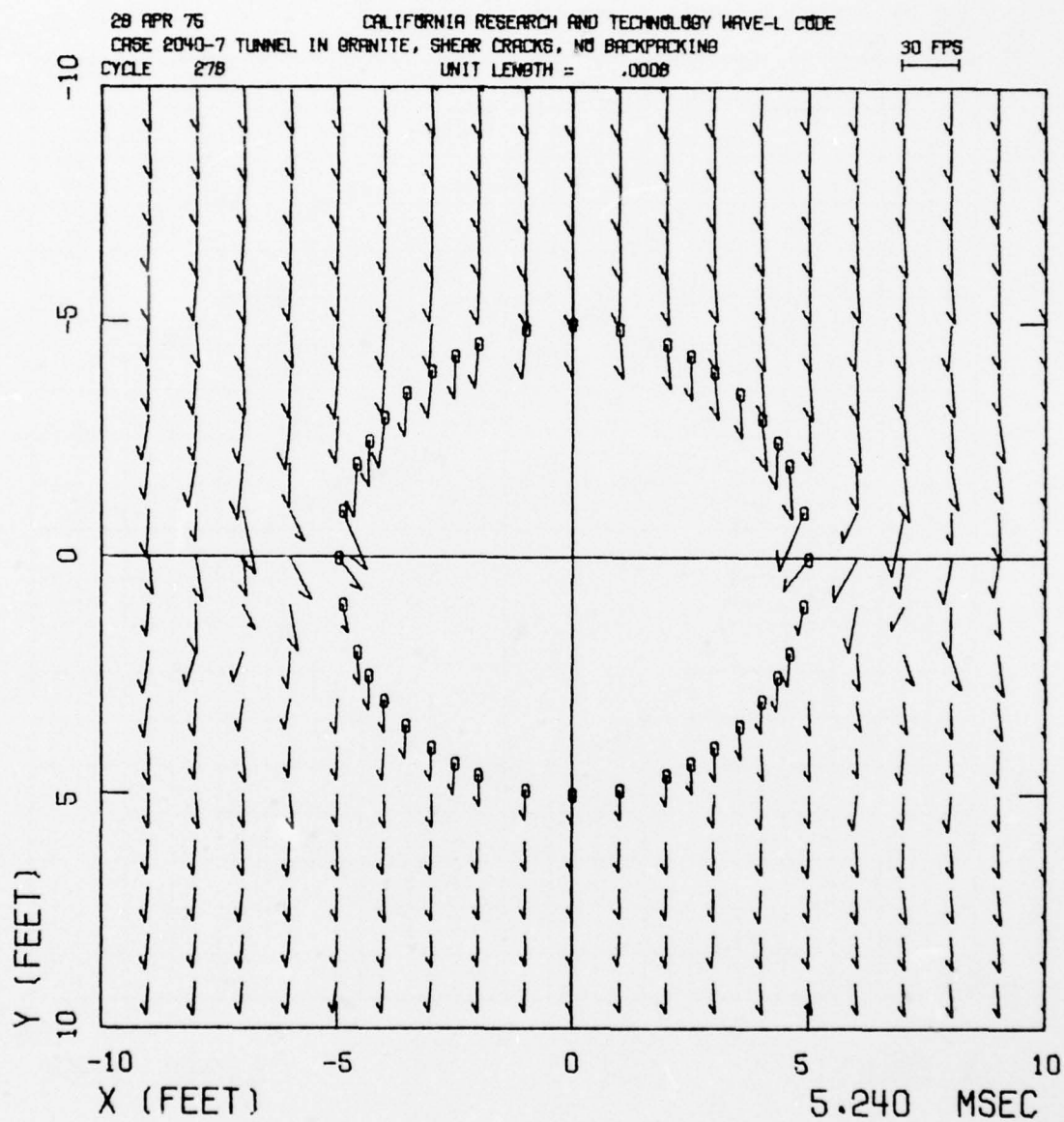



Figure 8. Case H - Unlined Tunnel in Granite with Explicit Shear Crack Model. Final Velocity Field (at 5.2 msec)



Principal stress vectors



in x-y plane  
in z direction

Vectors having rightward components are compressive; leftward vectors are tensile

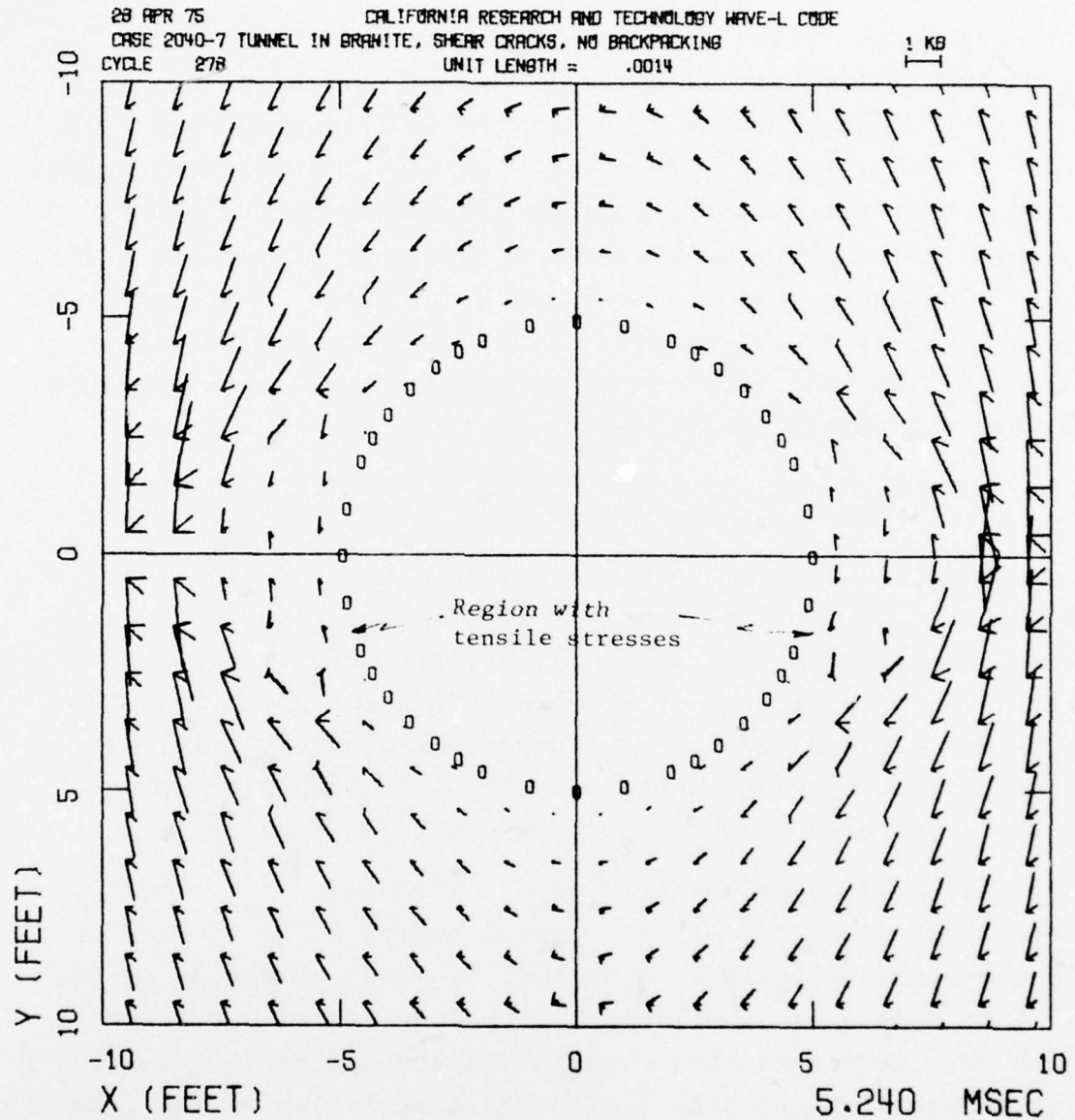


Figure 9. Case H - Unlined Tunnel in Granite with Explicit Shear Crack Model. Final Principal Stress Field (at 5.2 msec)

are developing in the regions where vertical cracks should initiate. These tensile stresses are of sufficient magnitude to produce cracking if a tensile failure model were present in this solution. This suggests that the vertical cracks which are observed experimentally are caused not by shear failure, as had been previously assumed, but by tensile failure. The stress relief allowed when the shear crack forms in the springline region produces tension in the surrounding material, and this tension can cause fractures which propagate to form the observed vertical cracks.

#### 4.2 CONCRETE LINERS IN TUFF - COMPARISONS SHOWING EFFECTS OF DIFFERENT FAILURE MODELS

Cases K and L examined the response of concrete liners in NTS tuff. Case K contained a 1-ft linear elastic concrete liner in tuff with the *plasticity* failure model. Case L contained the same liner, but the *explicit shear crack* failure model was used for the tuff. Comparison of the results from Cases K and L provides some indication of whether or not use of the more refined explicit crack model is necessary.

Figure 10 shows the grid used for these cases. The concrete liner is denoted by the shaded region. Figure 11 shows the computational grid in Case L at 10 msec, after the tunnel has been completely enveloped by the 1 kb stress wave. Cells which have developed shear cracks are denoted by the crossed line segments in the cells, with the orientation of the line segments indicating the directionality of the shear cracks. It is seen that most of the tuff cells in the problem have failed.

Figures 12 and 13 compare the stress fields for Cases K and L at 10 msec. Both of the failure models have resulted in

23 APR 75  
CASE 2040  
CYCLE

CALIFORNIA RESEARCH AND TECHNOLOGY WAVE-L CODE

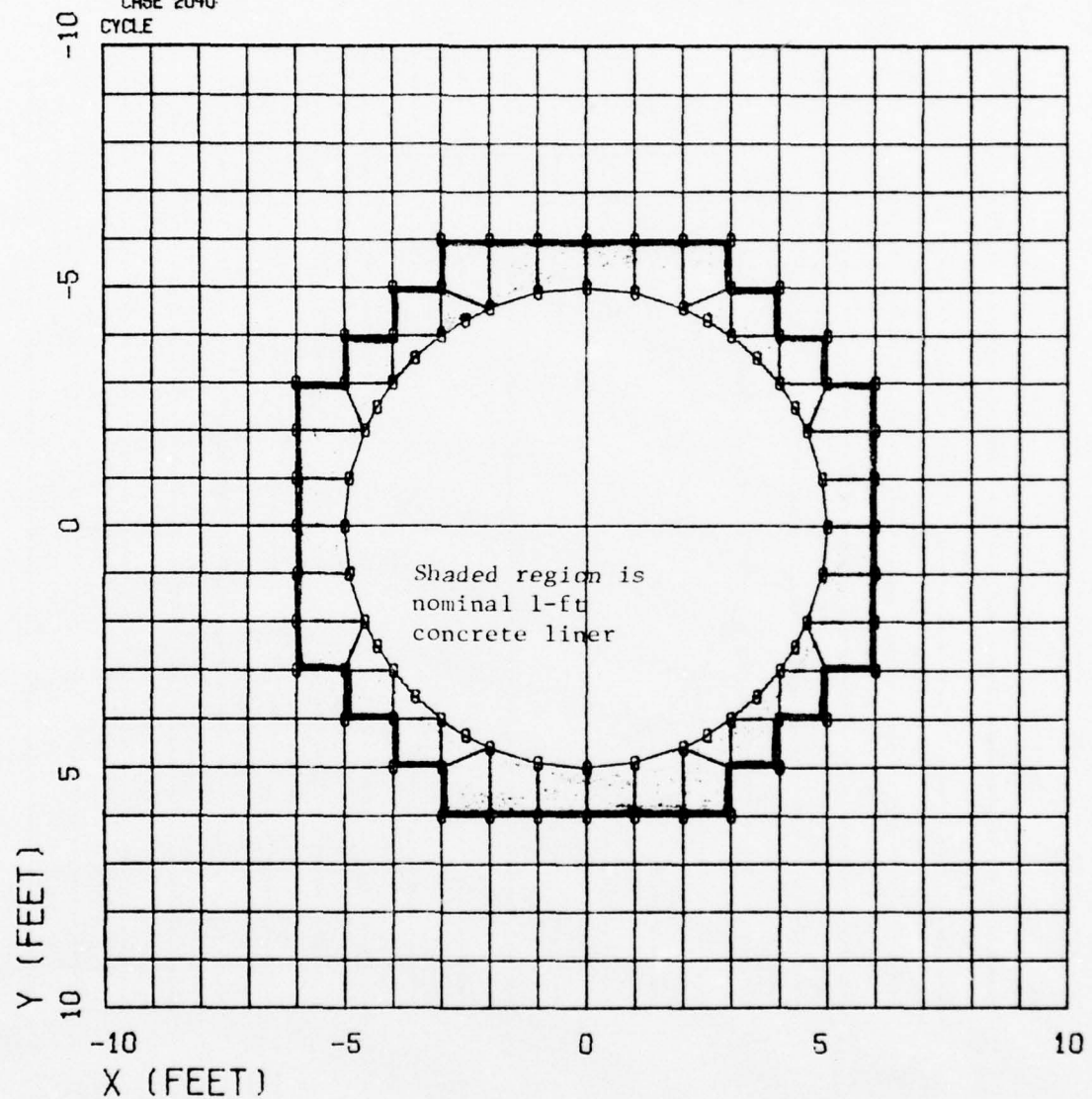


Figure 10. Computational Grid for Concrete Liners  
in Tuff (Cases K and L)

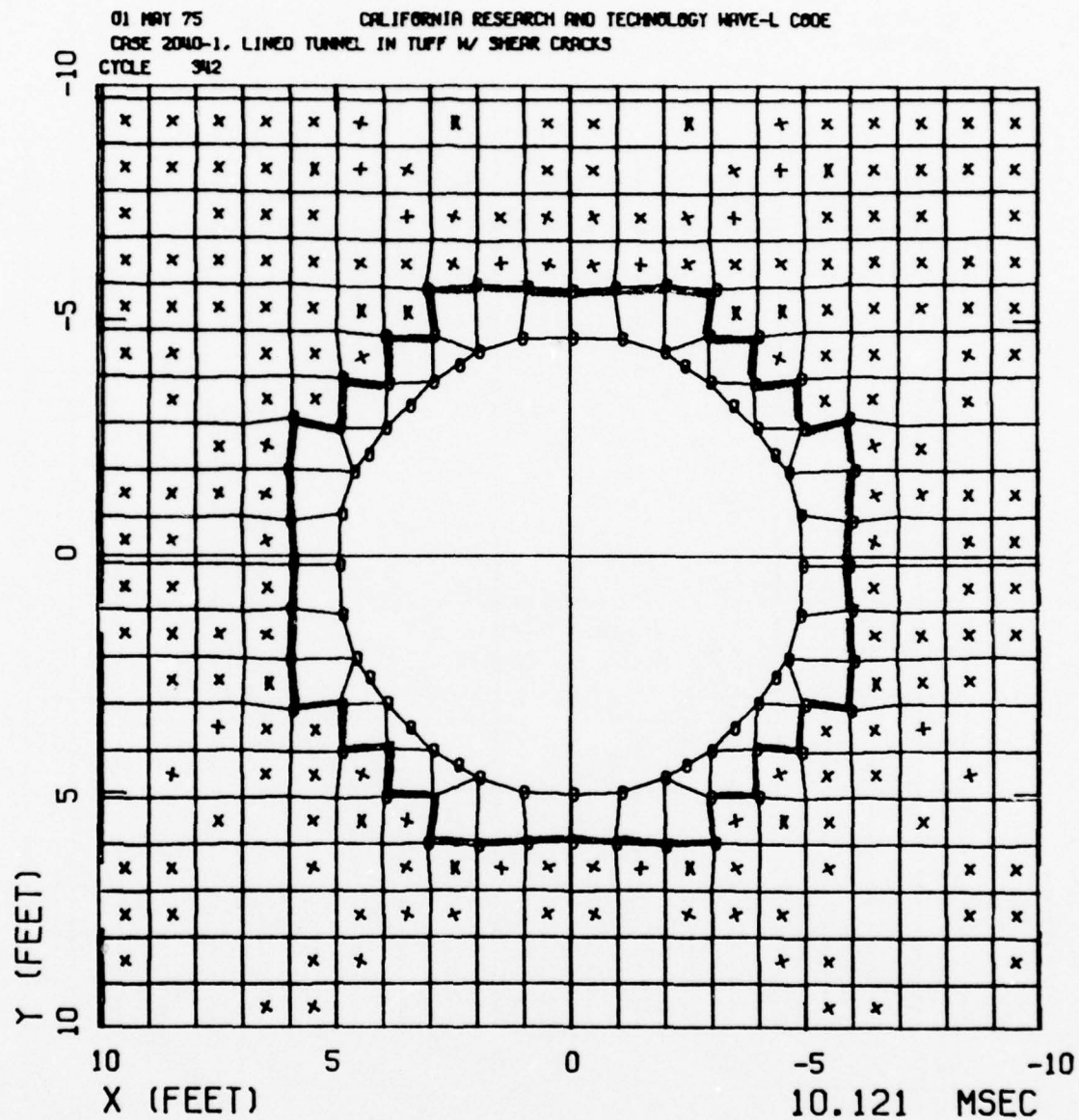


Figure 11. Case L - Concrete-Lined Tunnel in Tuff  
with Explicit Shear Crack Failure Model.  
Grid at 10.1 msec, Showing Pattern of  
Shear Cracks



Rightward components  
are compressive

Principal  
stress  
vectors

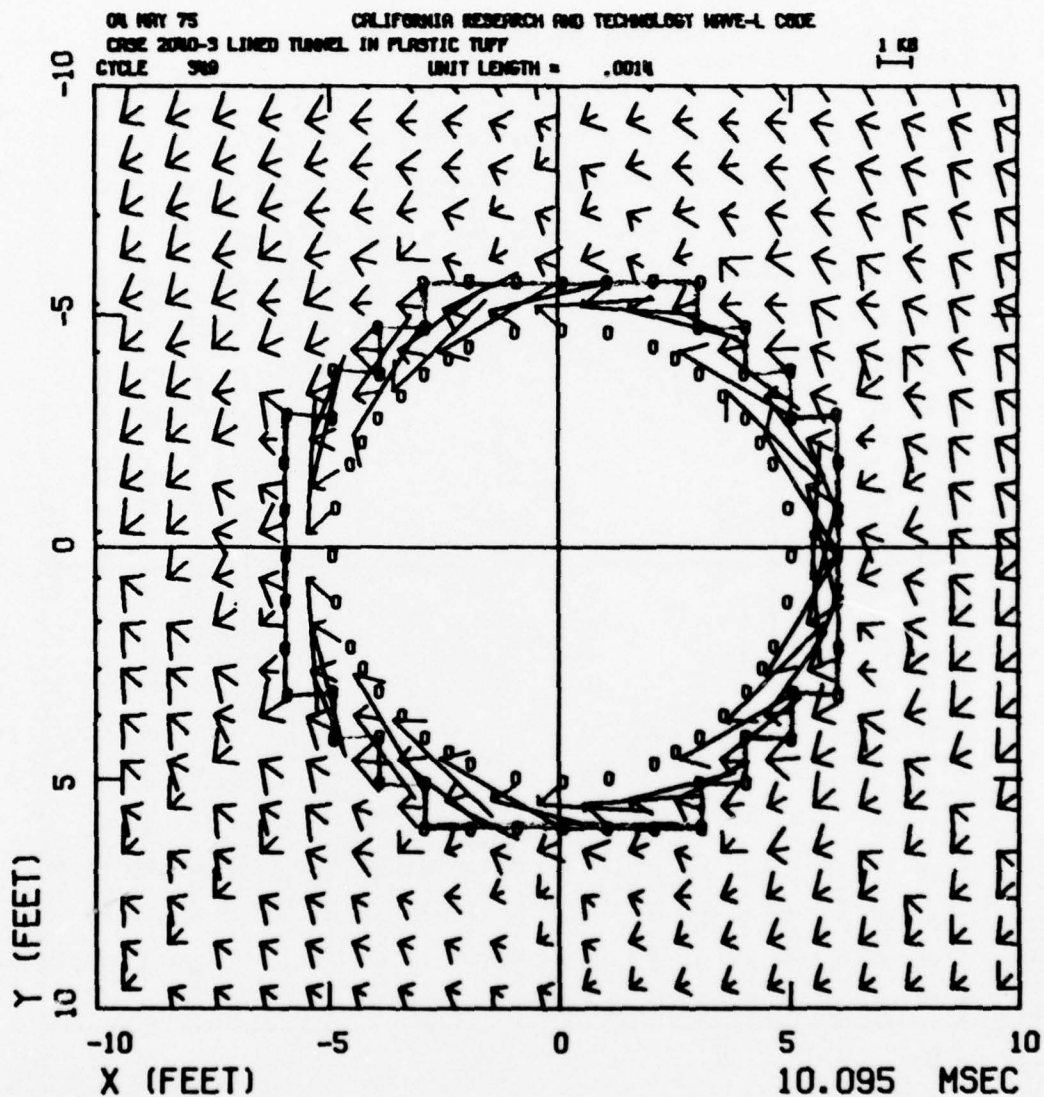
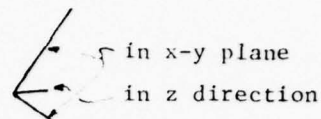


Figure 12. Case K - Concrete-Lined Tunnel in Tuff  
with Plasticity Failure Model.  
Principal Stress Field at 10.1 msec.

Rightward components  
are compressive

Principal  
stress  
vectors

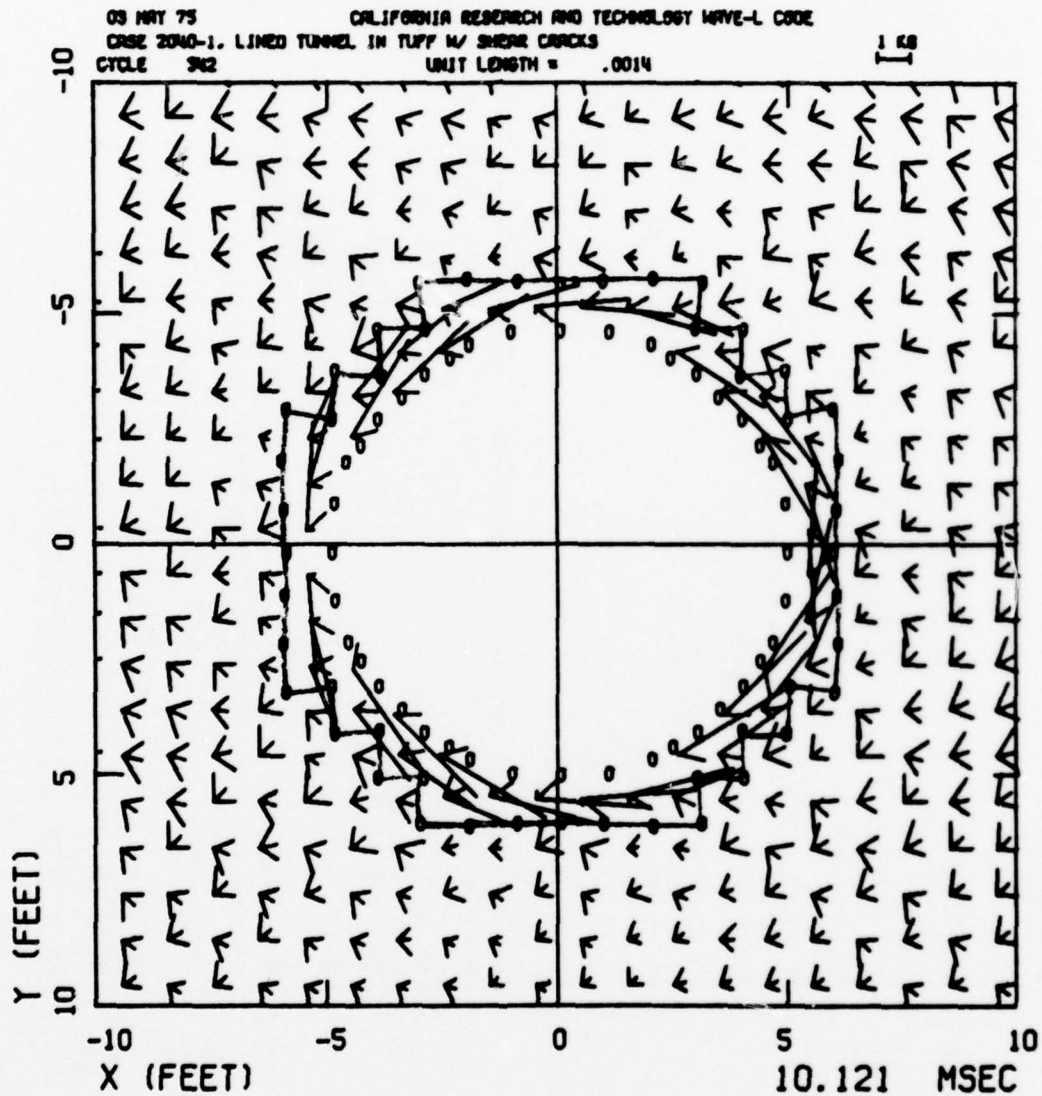
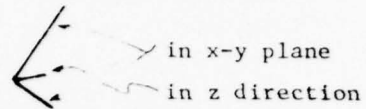


Figure 13. Case L - Concrete-Lined Tunnel in Tuff  
with Explicit Shear Crack Failure Model.  
Principal Stress Field at 10.1 msec.

essentially the same stress fields. The concrete liner in both cases has been compressed, producing a tangential (hoop) stress of about 3 kb. The principal stresses in the tuff are about 1 kb. Note that the principal stress components in the tuff adjacent to the liners are approximately equal, indicating that the liners are being subjected to a uniform pressure around their perimeters.

Figures 14 and 15 show the velocity fields for the two lined cases at 10 msec, and here we see that the two methods of treating failure have produced significant differences in the results. In Case K (Figure 14), the tunnel and backpacking have acquired a fairly uniform velocity, about the same as that of the surrounding tuff. In Case L (Figure 15), the explicit shear crack model has resulted in distinctly non-uniform velocities. In particular, note the large inward velocities on the tunnel-liner interface at about the 10:30 and 1:30 positions.

These comparative results indicate that the plasticity and explicit shear crack models for material failure may produce substantially different local velocities and hence displacements near the liner. In particular, the introduction of explicit shear cracks appears to lead to non-uniformities in the velocity field near the liner. This may cause stress concentrations which will need to be considered in the design of liners. To properly determine these concentrations, material models and numerical methods which allow the generation of discontinuities (i.e., both shear and tensile cracks) will be needed.

#### 4.3 UNLINED VS CONCRETE-LINED TUNNELS IN TUFF

Case J consisted of an unlined tunnel in tuff. The re-

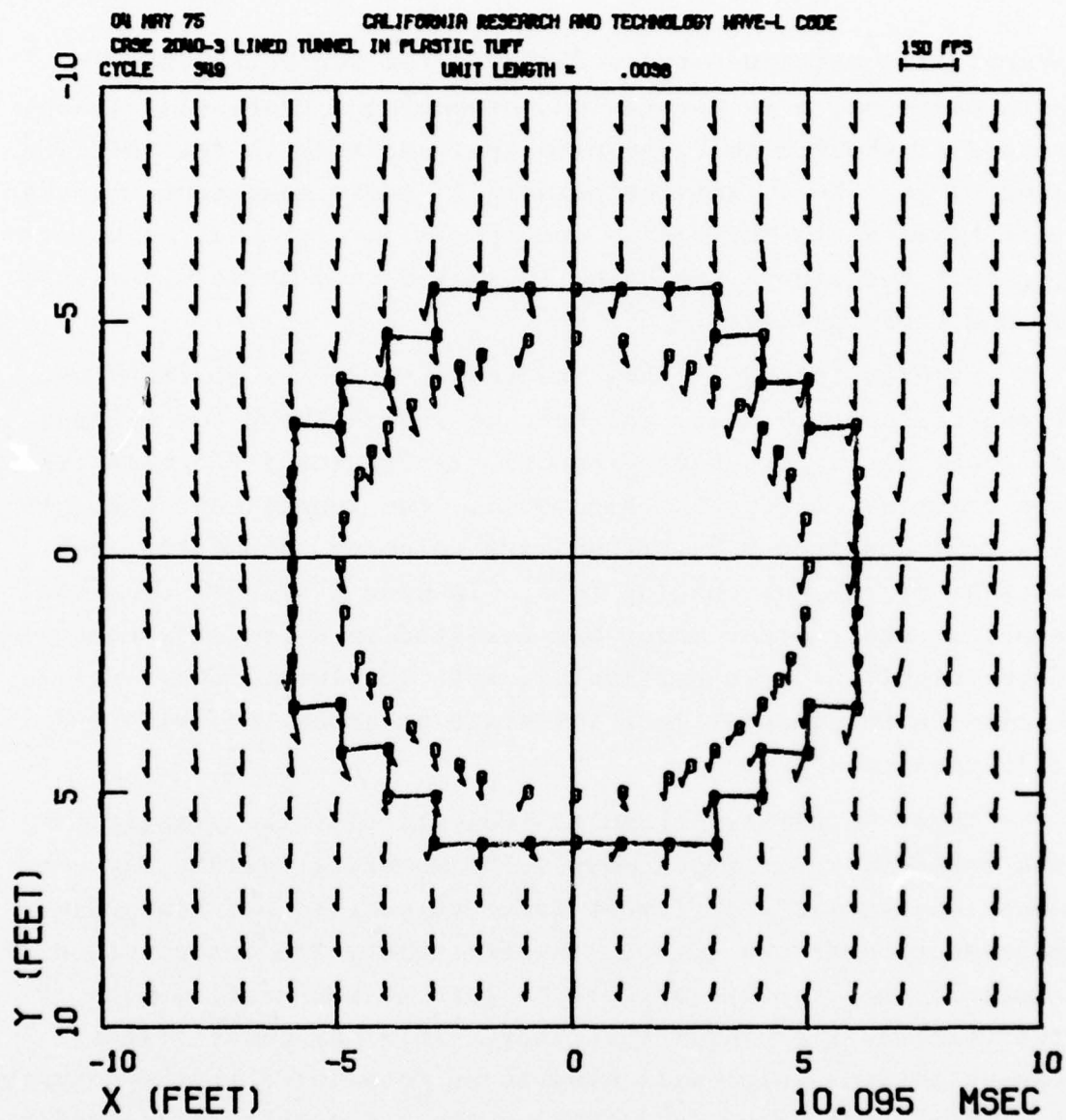


Figure 14. Case K - Concrete-Lined Tunnel in Tuff  
with Plasticity Failure Model.  
Velocity Field at 10.1 msec.



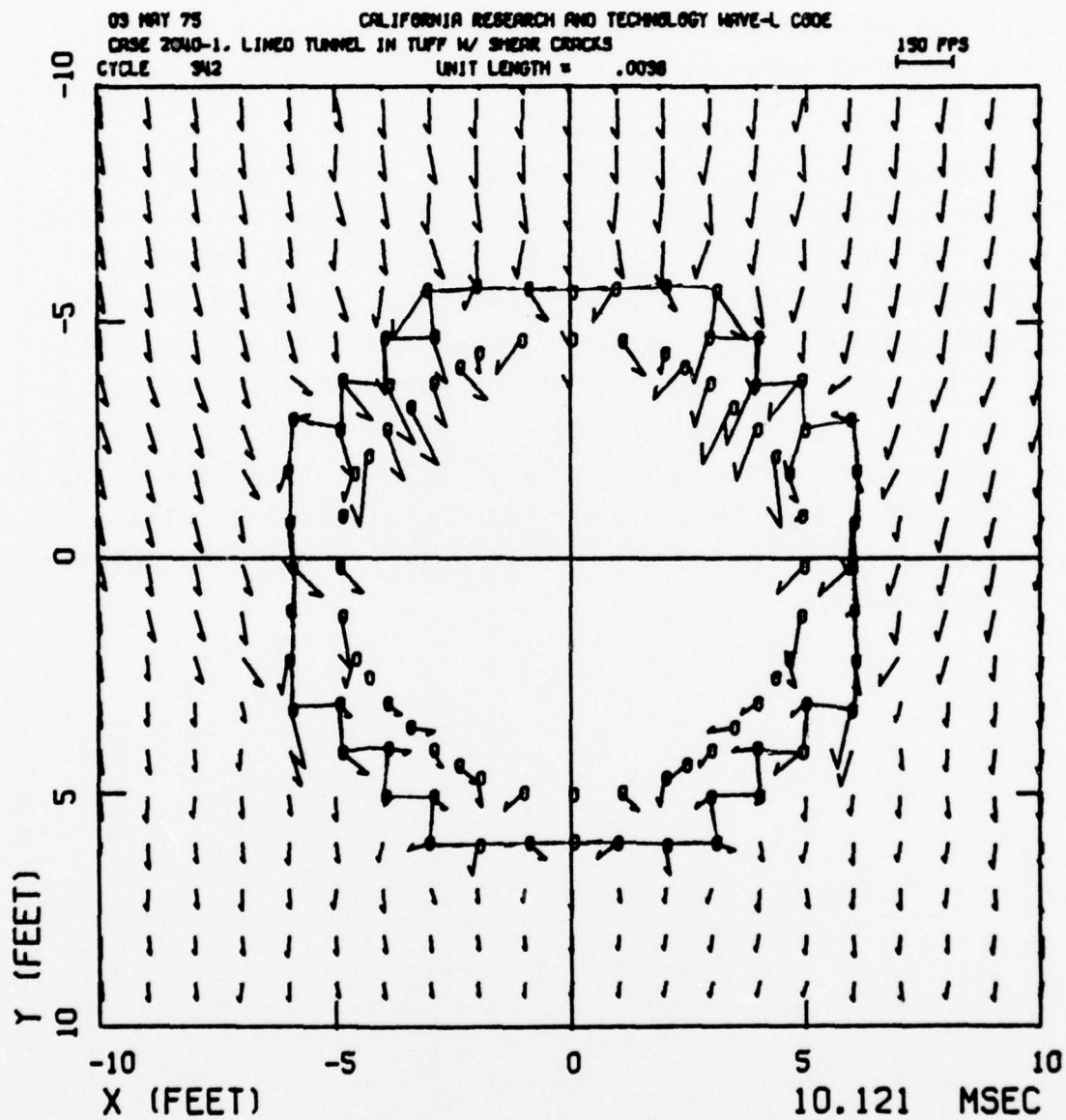


Figure 15. Case L - Concrete-Lined Tunnel in Tuff with Explicit Shear Crack Failure Model. Velocity Field at 10.1 msec.

sults can be directly compared with the preceding concrete-lined cases in tuff (Cases K and L) to show the action of the concrete liner.

Figures 16 and 17 show the stress and velocity fields for the unlined Case J at the same time as the corresponding plots for the lined cases (Figures 12-15). The unlined tunnel, rather than being accelerated to the velocity of the surrounding tuff, has developed significant inward velocities (at about twice the velocity of the surrounding tuff) and is collapsing. The strong tangential stresses which developed in the concrete liner (e.g., Figure 12) are totally missing in the tuff around the unlined tunnel (Figure 16). This tangential compression, of course, is what prevents the collapse of lined tunnels.

Rightward components  
are compressive

Principal  
stress  
vectors

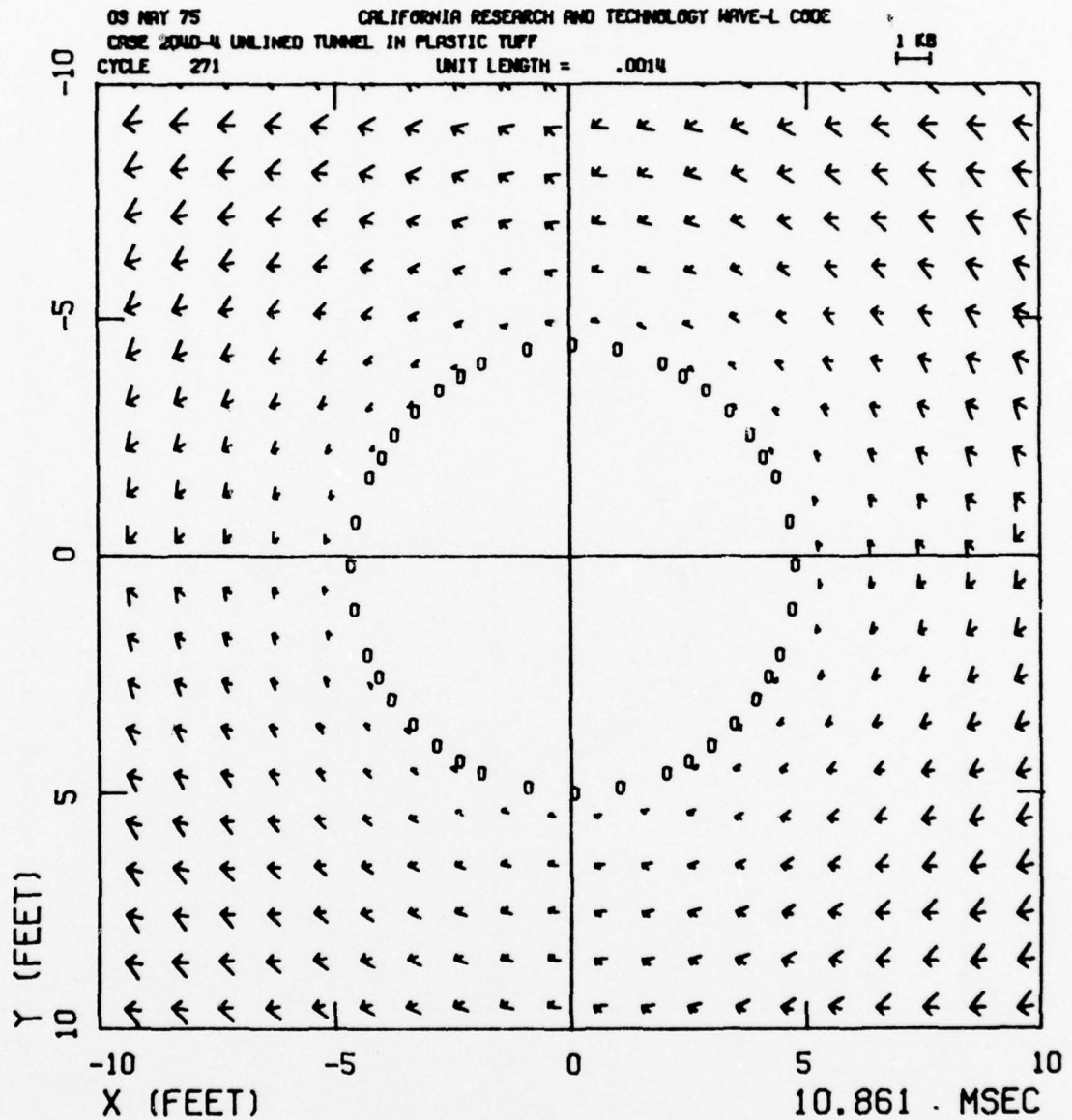
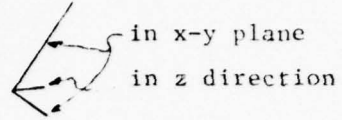


Figure 16. Case J - Unlined Tunnel in Tuff  
with Plasticity Model. Principal  
Stress Field at 10.9 msec.

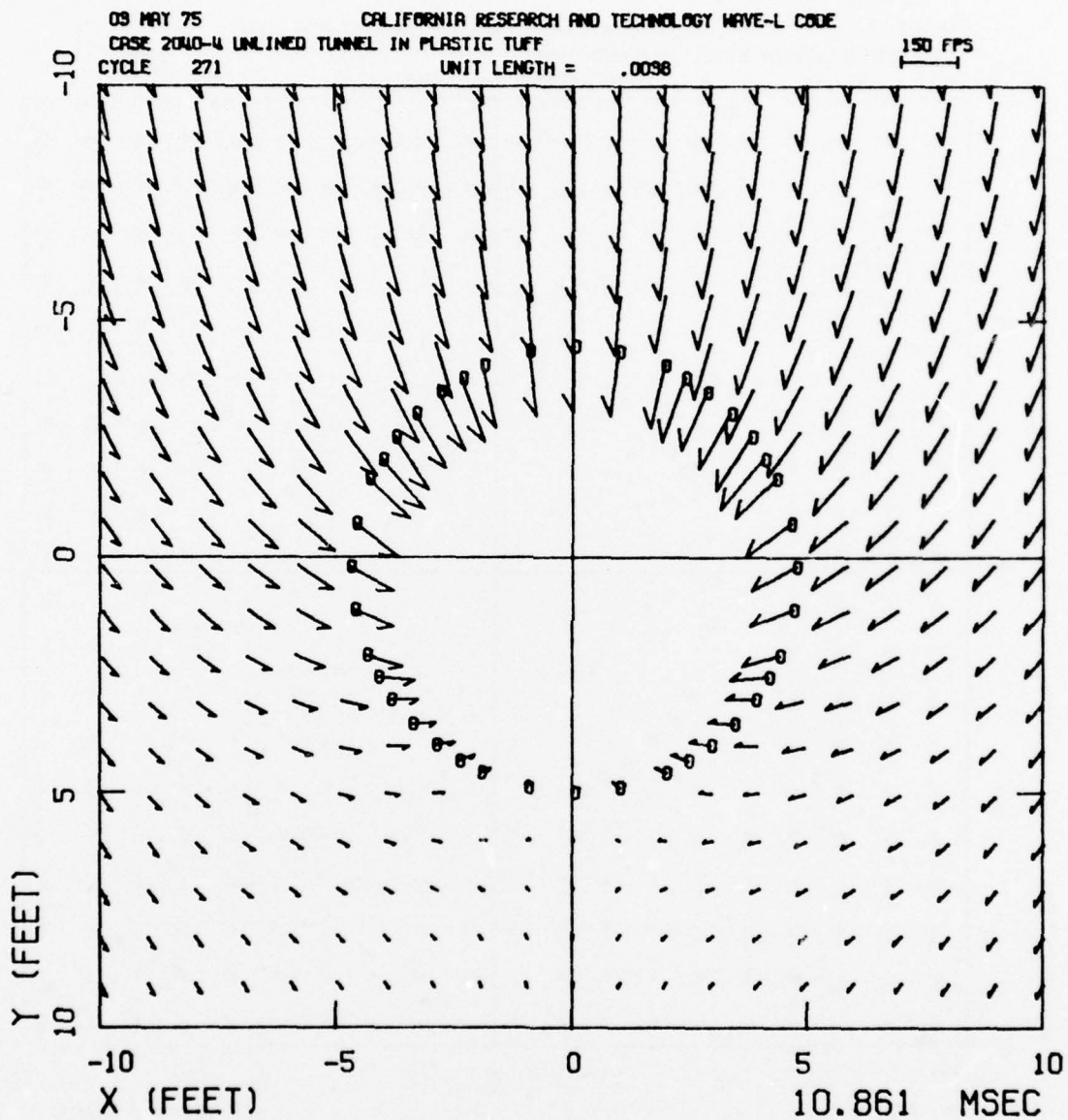


Figure 17. Case J - Unlined Tunnel in Tuff  
with Plasticity Failure Model.  
Velocity Field at 10.9 msec.



## 5. COUPLED FINITE DIFFERENCE/FINITE ELEMENT LAP CODE FOR ANALYSIS OF THIN LINERS

Thick liners can be represented using a finite difference code, as is seen by the examples in Cases K and L in Section 4.2 above. It is not practical, however, to treat thin liners, such as steel, by the finite difference method because relatively small cells must be used to resolve action in the thin steel section. The combination of small cells and high sound speed in steel lead to time steps which are too small for fairly long-duration buried structure analyses.

For convenience, steel liners are sometimes represented as rigid bodies in buried structure analyses. This was the approach taken in Phase I of this study. It is a reasonable approach so long as elastic distortion of the liner does not cause substantial stress adjustments, or allow small joint motions in the nearby medium. Unfortunately, test results indicate that elastic diametral strains are indeed sufficient to be of concern in analyses of integral liners. Thus blocks which are in contact with integral liners may be able to shift slightly, producing non-uniform stresses along the medium/liner interface, and perhaps substantial stress concentrations in the liner. These will need to be taken into consideration in the design of integral liners.

Our approach to this problem has been to implement a coupled finite difference/finite element numerical method, which we will call LAP, for Linked Analysis Program. In this coupled method, the earth medium is represented by the Lagrangian finite difference WAVE-L code, which allows joint slippage and stress accommodations to occur around the liner, and which treats the far field and near field ground motions in

efficient manner. The integral structural liner is represented by an adaptation of the finite element SAP IV code<sup>6</sup>, which can describe the displacements of the liner and the dynamics of the stress field in the liner. Concrete backing for a steel liner can be treated using either the finite element or the finite difference portion of the LAP method.

The finite difference and finite element portions of LAP are coupled on a cycle-by-cycle basis across a specified interface (usually the medium/liner interface). In each integration cycle, the finite difference code provides forces across the interface to the finite element code, which in turn provides displacements back across the interface. This linked LAP method is now operational, and it was used to generate the solutions with steel liners (Cases M and N) which are described in the following section.

## 6. DEFORMABLE STEEL LINERS

For the initial LAP code analyses, two solutions were obtained for steel liners in tuff (Cases M and N). In both of these cases, two-inch thick steel liners were used in a 10-ft dia tunnel in tuff. The steel was considered to be linearly elastic (i.e., with no yield or failure criterion). The tuff was modeled using the explicit shear crack failure model described in Section 3.

The liner was represented in the finite element portion of the LAP code by 32 beam finite elements, coupled to the finite difference cells at the interface node points.

### 6.1 TWO-INCH STEEL LINER IN TUFF (CASE M)

In this problem, the steel liner was in direct contact with the tuff medium. The solution was run to 15 msec. Figures 18, 19, and 20 show the computational grid velocity field, and principal stress fields at 7.5 msec, as the stress wave is engulfing the tunnel. Figures 21, 22, and 23 show the same plots at 14.5 msec, with the tunnel completely engulfed by the step wave. The pattern of shear cracks is similar to that obtained in the earlier solution of a concrete liner in tuff (Case L, Figure 11).

Time histories of the steel liner response were obtained from the finite element portion of LAP at the stations identified in Figure 24. Figures 25 to 29 show the hoop stress histories on the inner surface (i.e., the free surface) and on the outer surface (the steel/tuff interface). These stresses exceed a nominal yield strength of steel (say 10 kb, or 150 ksi) after about 12 msec, so permanent deformation and probably failure of the liner will occur. At the end of the solution

at 15 msec, the hoop stress is beginning to level off as it approaches about 30 kb (450 ksi), which would be the stress level reached in a static solution of this problem.

Figures 30 to 35 show displacement and velocity histories at the top and bottom stations, and at the springline of the liner. The vertical displacements and velocities are relative to the center of mass of the steel liner. Note that the top station (25) has been pushed down towards the center of mass about 4 inches by 15 msec. The bottom station (9) first moves up, relative to the mass center, then also moves downward, to about 1 inch by 15 msec. The springline station (1) experiences about 1-in outward radial displacement by 15 msec (about 2-in diametral strain). These motions occur at velocities, relative to the center of mass, in the range up to about 150 fps. Slopes of the velocity histories indicate relative accelerations of the order of 1000-3000 g's.

#### 6.2 TWO-INCH STEEL LINER BACKED BY TWO FEET OF CONCRETE IN TUFF (CASE N)

This problem was identical to the preceding Case M, except that the steel liner was backed by about two feet of concrete. The concrete was treated by the finite difference portion of the code, so the finite difference/finite element interface was between the steel liner and the concrete. Figure 36 shows the computational grid at 7.5 msec, as the stress wave was engulfing the tunnel. The concrete backing is shown by shading in this plot. Figure 37 and 38 show the velocity and principal stress fields at this same time.

The solution was carried out until 9.5 msec, and the final grid, velocity field, and principal stress field are shown in Figures 39, 40, and 41. The stress level in the concrete had reached about 3-4 kb by this time, and was beginning to rise



sharply in the steel. We did not continue the solution further.

An alternative to placing the finite difference/finite element interface between the steel and concrete would be to include the concrete in the finite element portion of the solution. This would be somewhat more efficient, but it would sacrifice the generality in treatment of material properties, fracture, and explicit crack propagation which is available in the finite difference code.

## REFERENCES

1. S. E. Blouin, "Data Report, DATEX II", AFWL-TR-69-149, January 1970
2. M. Rosenblatt and K. N. Kreyenhagen, "Free Field Motions in Jointed Media", DNA 2769F, November 1971
3. S. W. Butters, R. J. Reid, S. J. Green, and A. H. Jones, "Mechanical Properties of Nevada Test Site Tuffs from Selected Exploratory Drill Holes", DNA 3181F, September 1973
4. K. Goering, DNA/SPSS, Personal Communication
5. T. C. Kennedy and J. V. Zaccor, "Theoretical and Laboratory Investigation of Deep Based Structures", Progress Reports on SRI Project 3743, 1974
6. K.-J. Bathe, E. L. Wilson, and F. E. Peterson, "SAP IV, A Structural Analysis Program for Static and Dynamic Response of Linear Systems", EERC 73-11, Earthquake Engineering Research Center, Univ. of California, Berkeley, April 1974

29 JUN 75 CALIFORNIA RESEARCH AND TECHNOLOGY  
CASE LAP-2040-M STEEL LINED TUNNEL IN TUFF WITH SHEAR CRACKS  
CYCLE 150

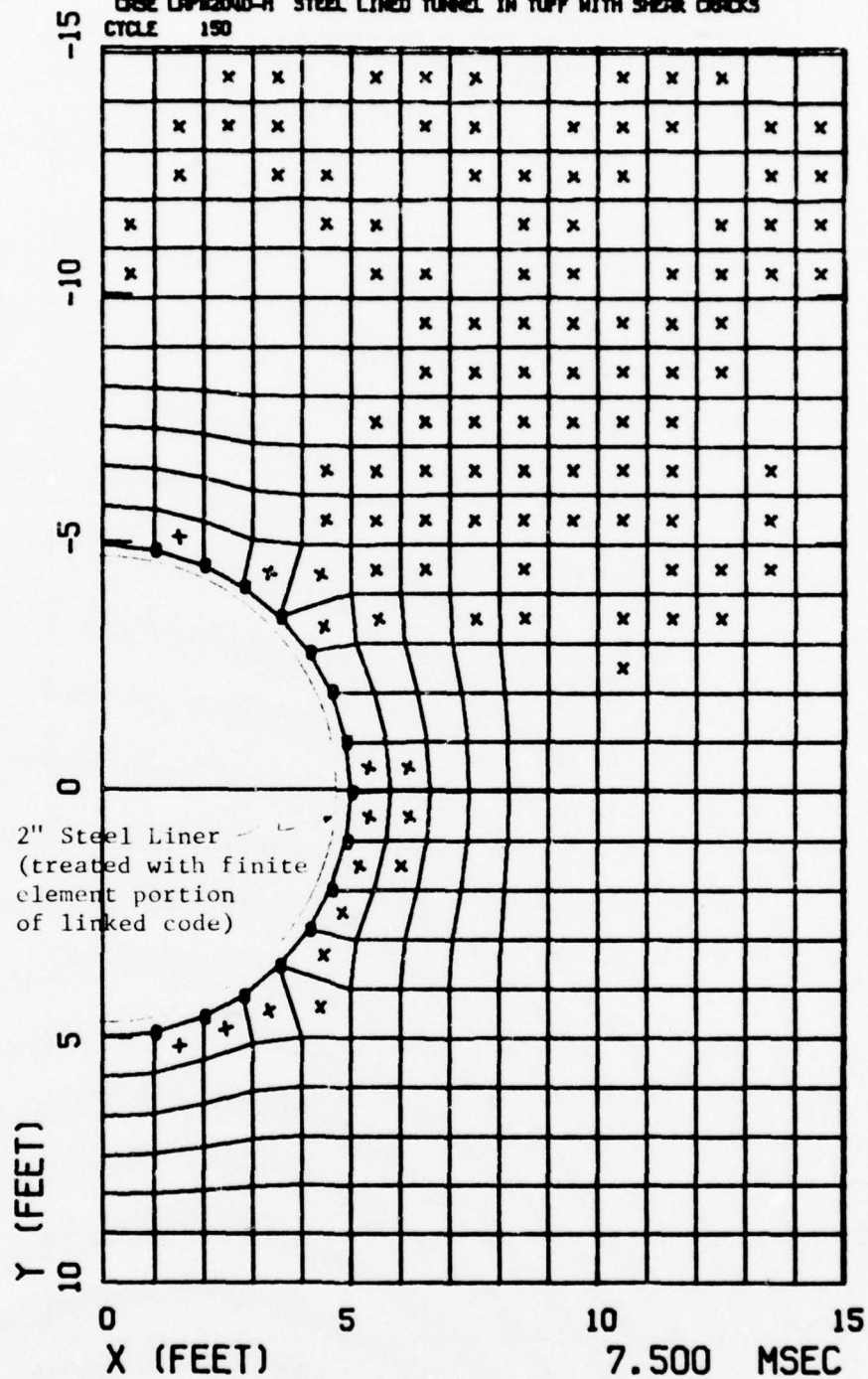


Figure 18. Computational Grid for Lagrangian Finite Difference Portion of LAP Code Solution for Case M - 2" Steel Liner in Tuff with Explicit Shear Crack Failure Model. (t = 7.5 msec)

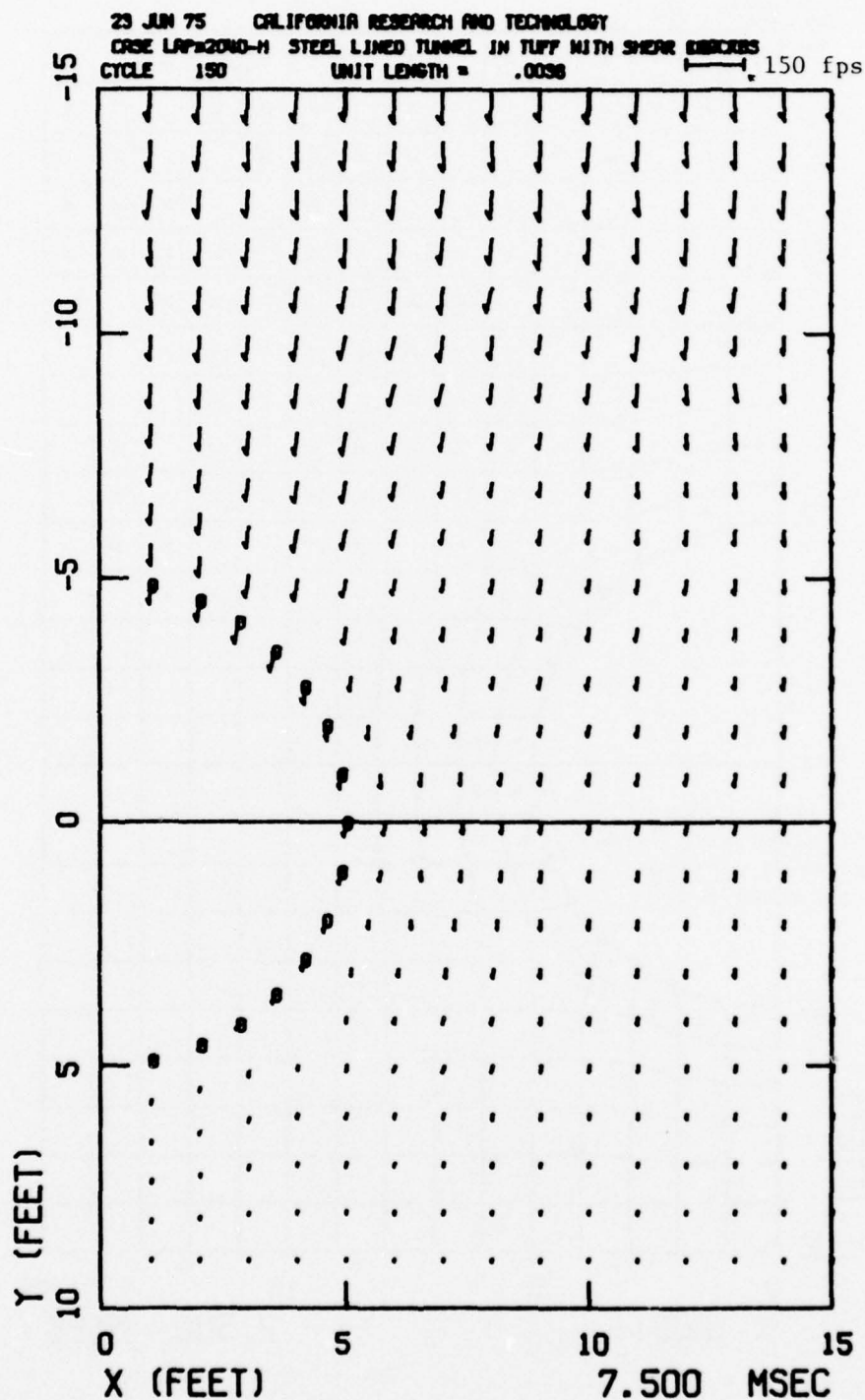


Figure 19. Velocity Field for Lagrangian Finite Difference Portion of LAP Code Solution for Case M - 2" Steel Liner in Tuff with Explicit Shear Crack Failure Model ( $t = 7.5$  msec)



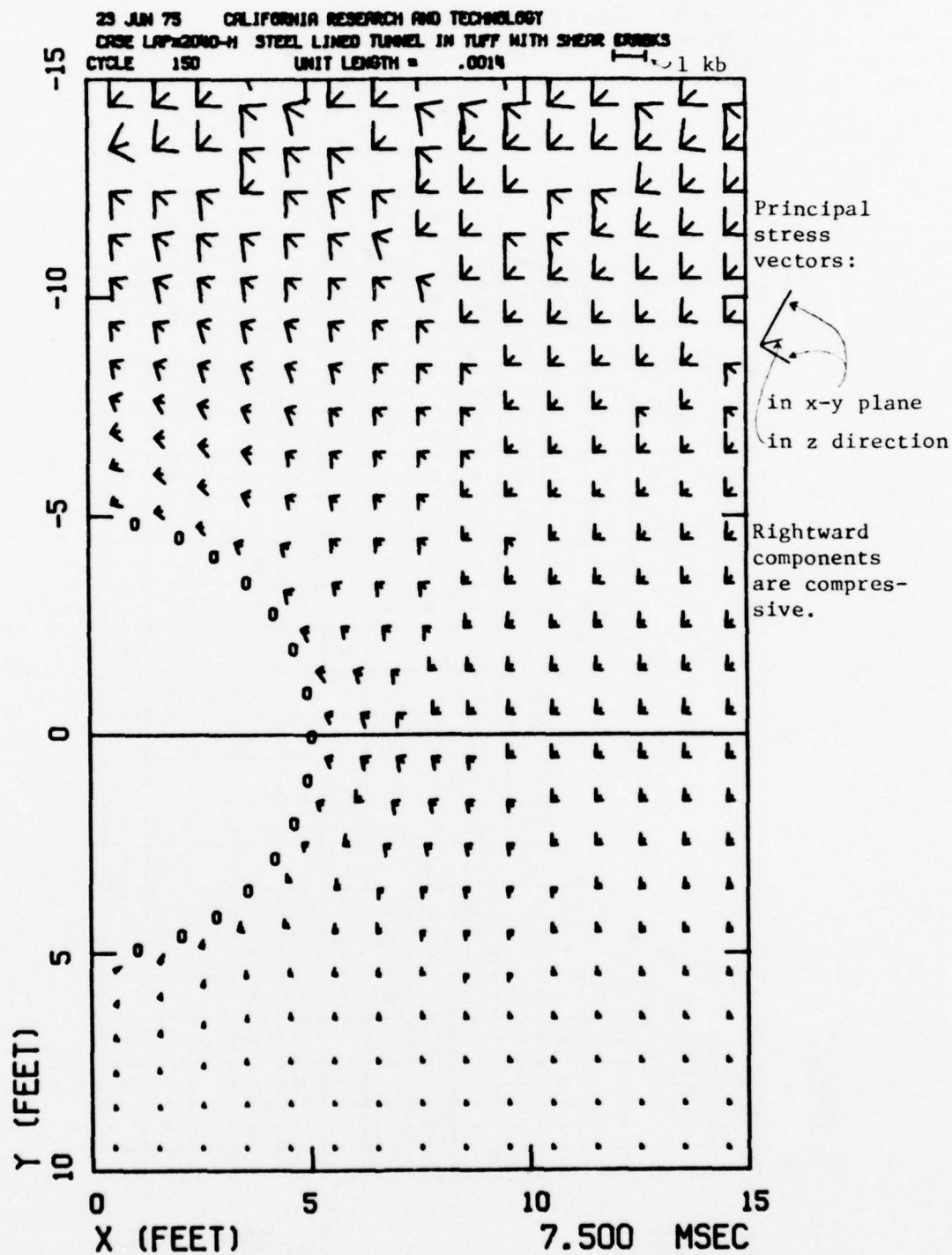


Figure 20. Principal Stress Field for Lagrangian Finite Difference Portion of LAP Code Solution for Case M - 2" Steel Liner in Tuff with Explicit Shear Crack Failure Model. ( $t = 7.5 \text{ msec}$ )

21 JUN 75 CALIFORNIA RESEARCH AND TECHNOLOGY  
CASE LAP#2040-M STEEL LINED TUNNEL IN TUFF WITH SHEAR CRACKS  
CYCLE 280

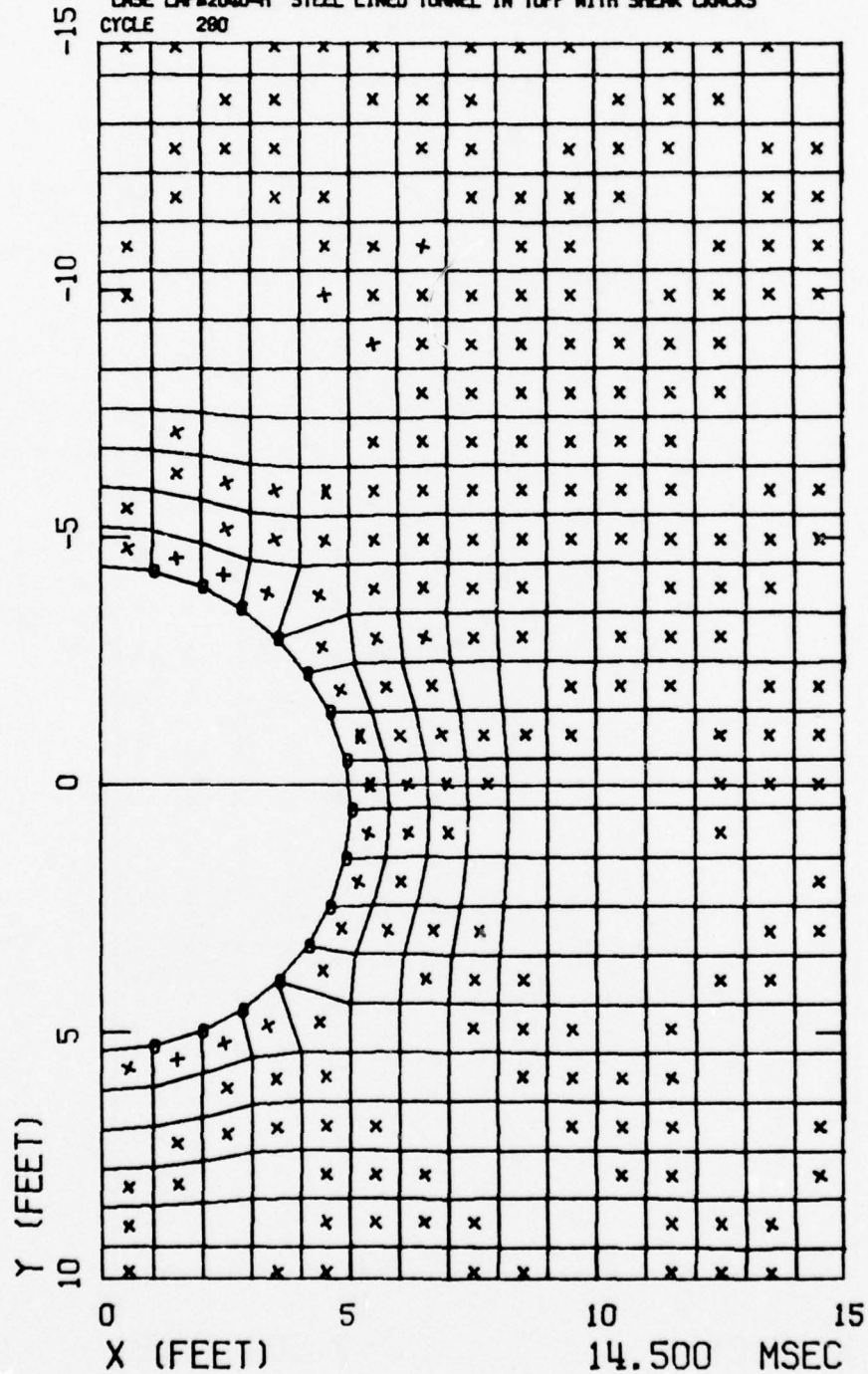


Figure 21. Computational Grid for Lagrangian Finite Difference Portion of LAP Code Solution for Case M - 2" Steel Liner in Tuff with Explicit Shear Crack Failure Model ( $t = 14.5$  msec)

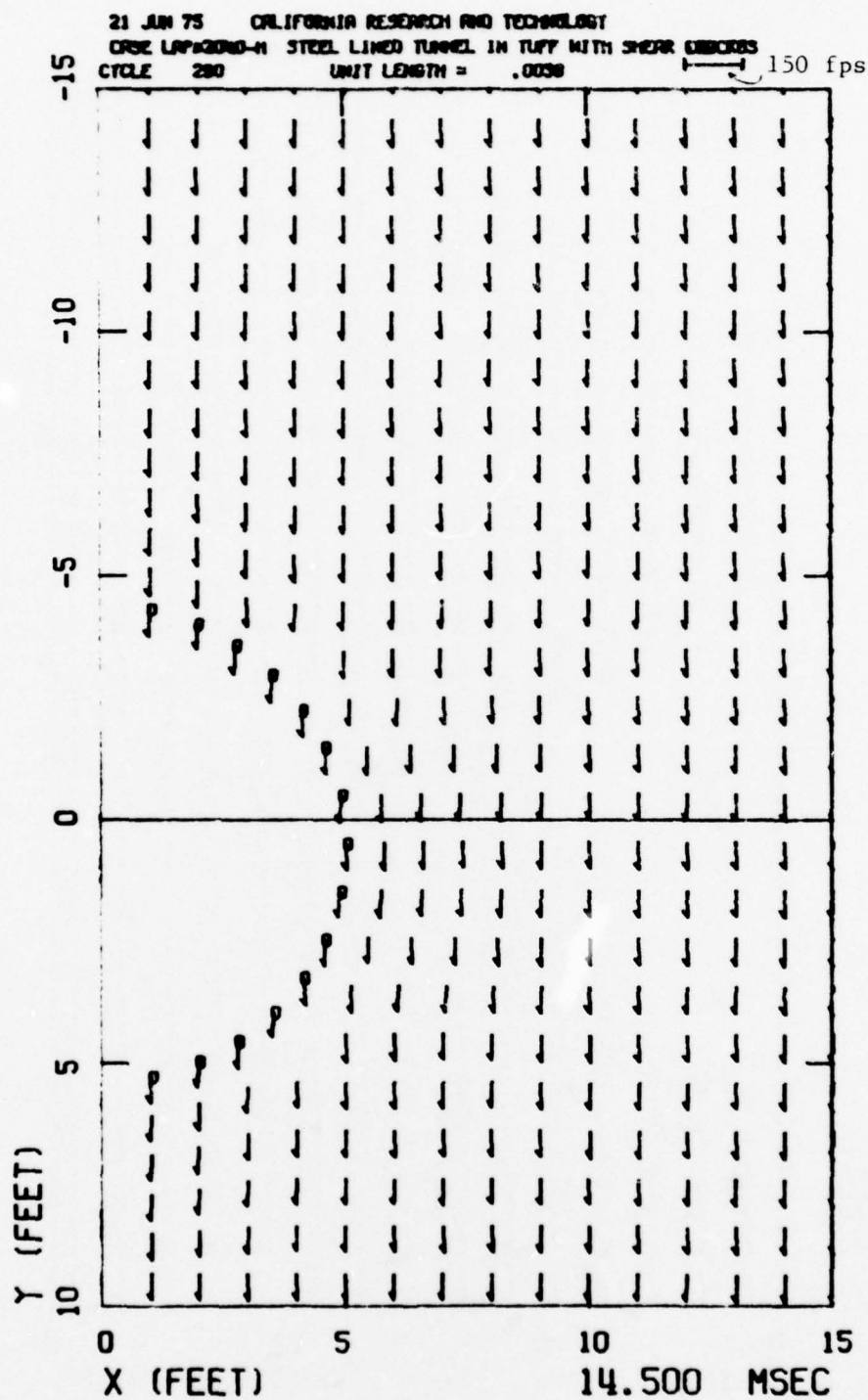


Figure 22. Velocity Field for Lagrangian Finite Difference Portion of LAP Code Solution for Case M - 2" Steel Liner in Tuff with Explicit Shear Crack Failure Model ( $t = 14.5$  msec)

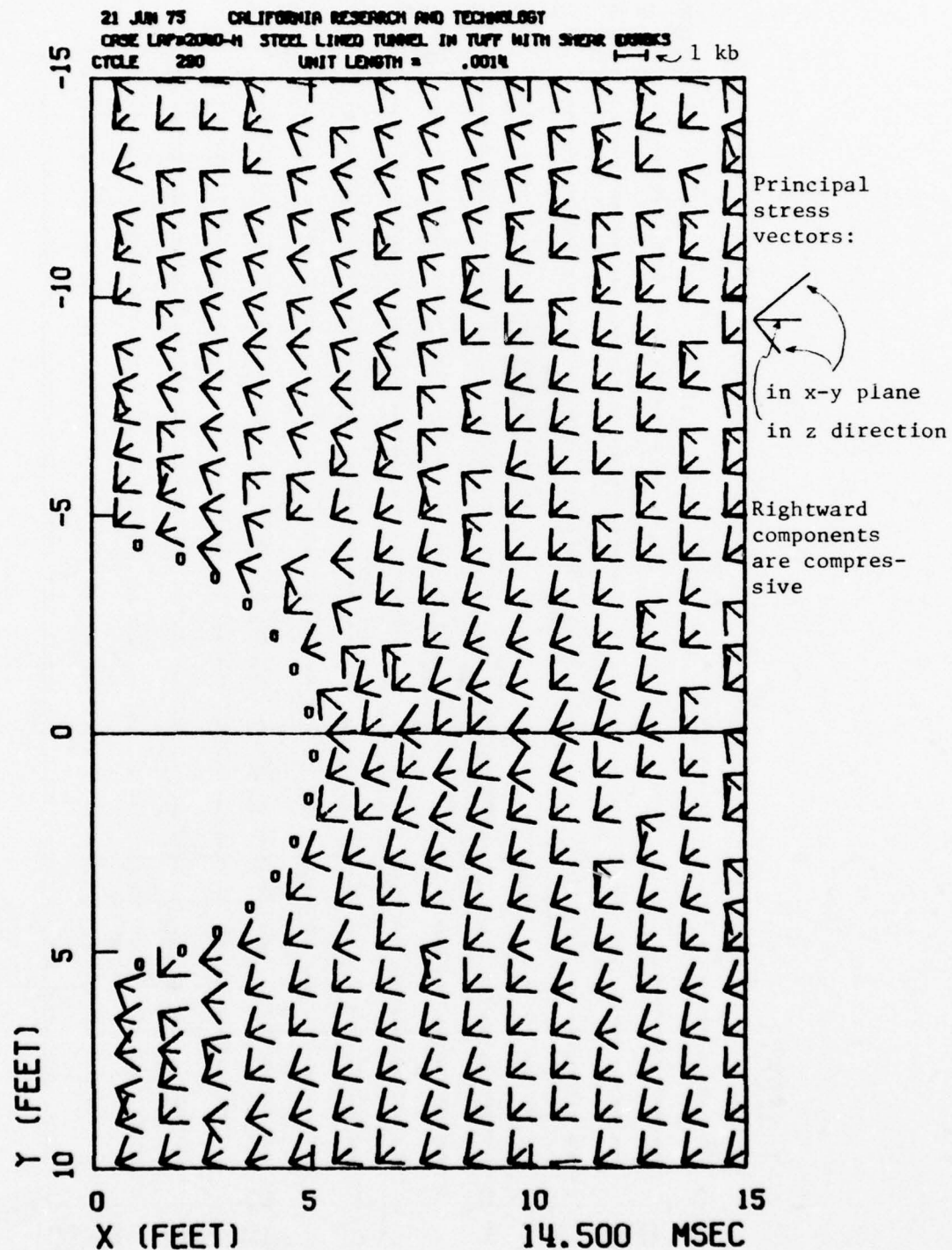


Figure 23. Principal Stress Field for Lagrangian Finite Difference Portion of LAP Code Solution for Case M - 2" Steel Liner in Tuff with Explicit Shear Crack Failure Model. ( $t = 14.5$  msec)



19 JAN 75 CALIFORNIA RESEARCH AND TECHNOLOGY  
 LAPA2040-M STEEL LINED TUNNEL IN TUFF WITH SHEAR CRACKS  
 CYCLE 0

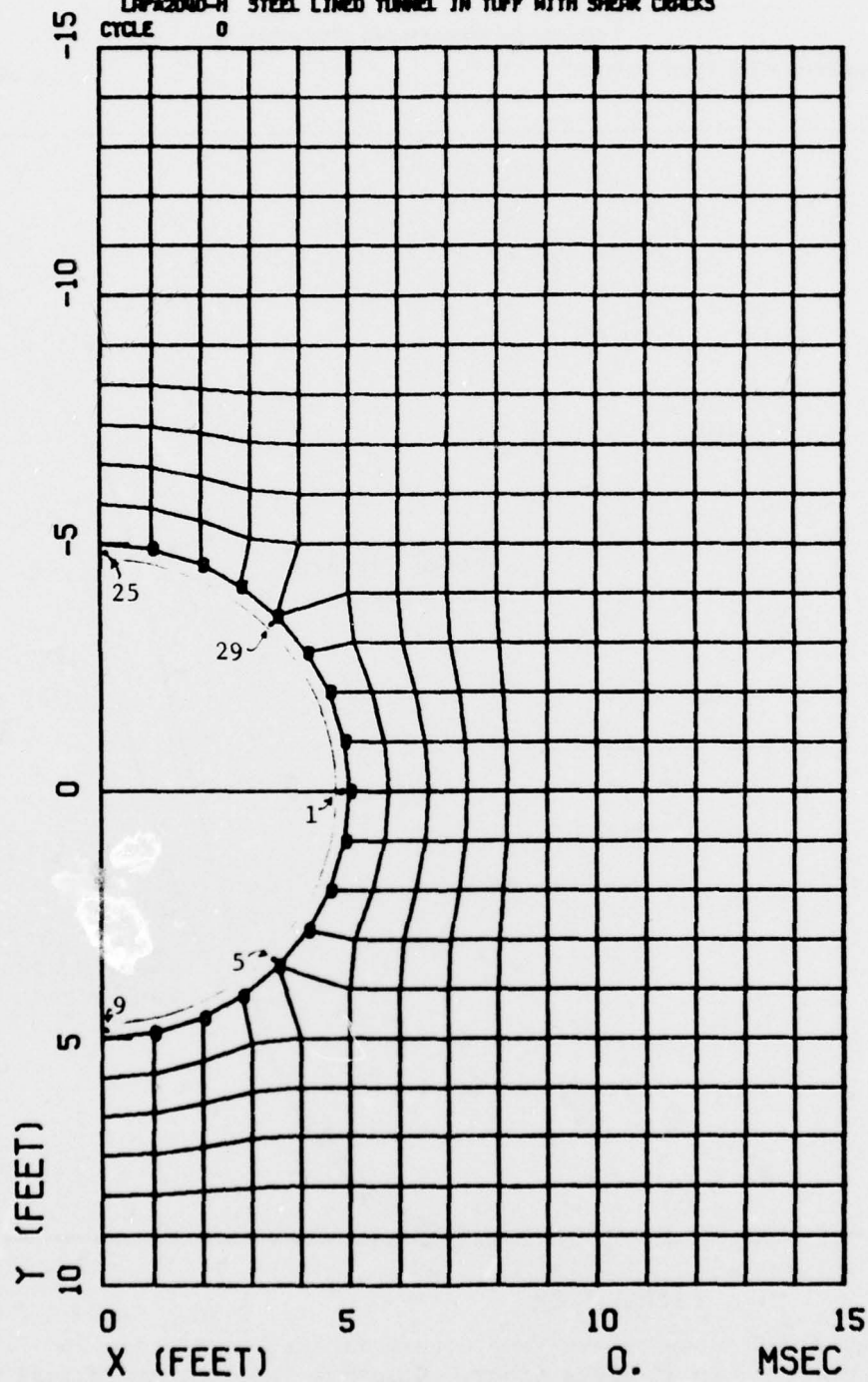


Figure 24. Locations of Time-History Stations for  
 Plots in Figures 25-29 (Case M - 2" Steel  
 Liner in Tuff)

CALIFORNIA RESEARCH AND TECHNOLOGY, INC.

LAP-2000-H STEEL LINER RESPONSE

23 JUN 75

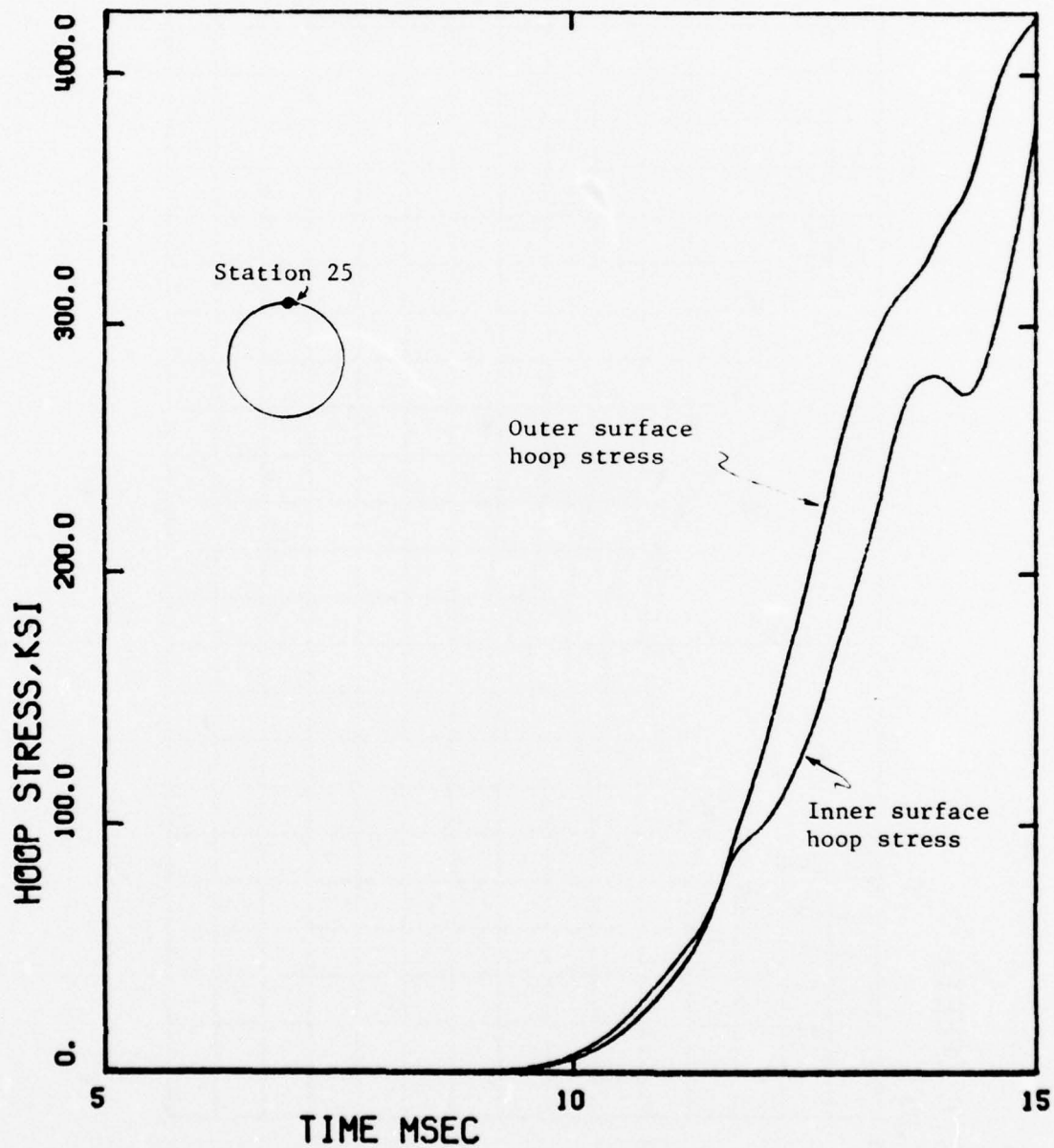


Figure 25. Compressive Hoop Stress History at Station 25 in 2" Steel Liner. Case M - Steel Liner in Tuff

CALIFORNIA RESEARCH AND TECHNOLOGY, INC.

LAP-2010-H STEEL LINER RESPONSE

23 JUN 75

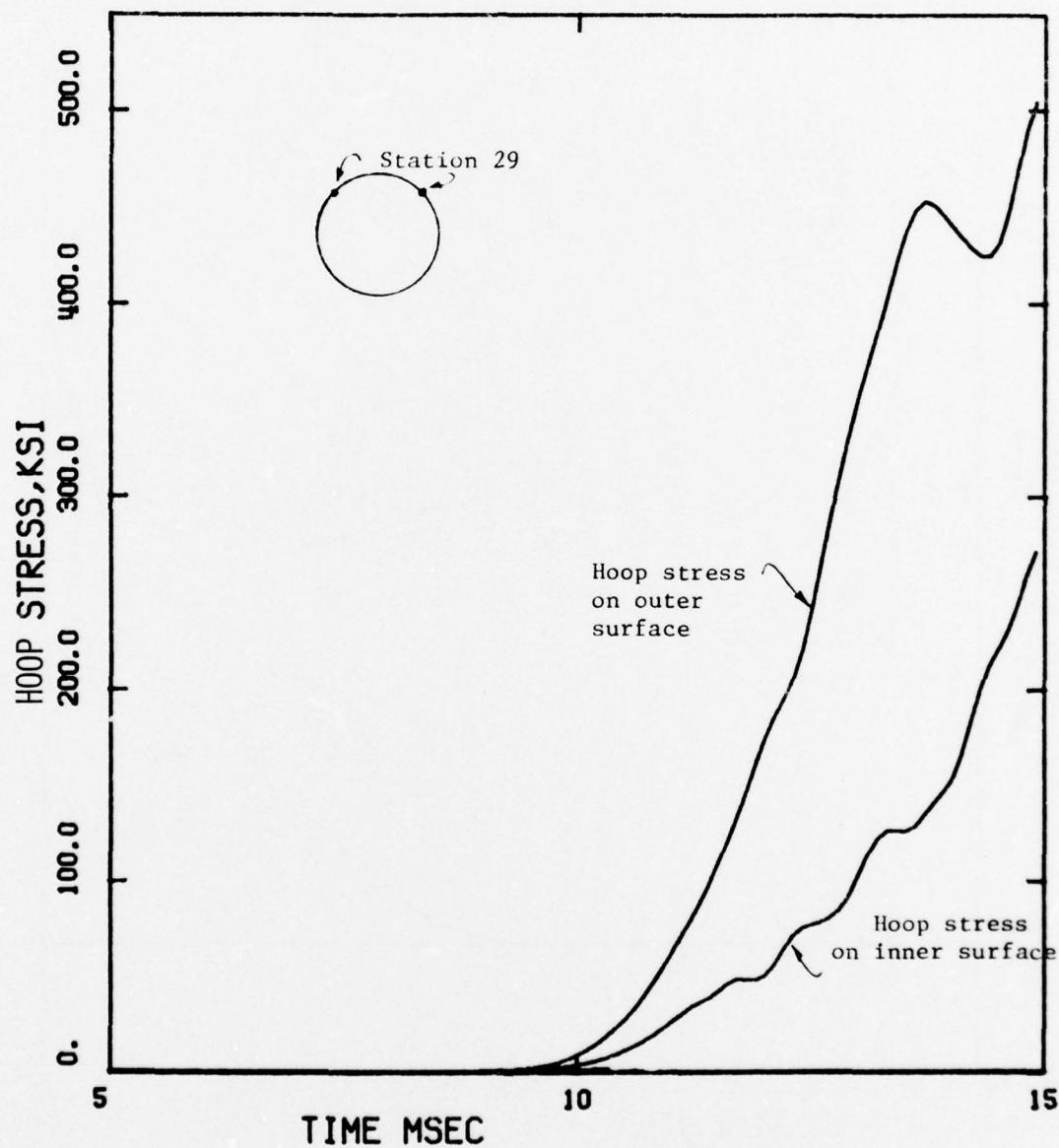


Figure 26. Compressive Hoop Stress History at Station 29 in 2" Steel Liner. Case M - Steel Liner in Tuff

CALIFORNIA RESEARCH AND TECHNOLOGY, INC.

LAP-2010-H STEEL LINER RESPONSE

23 JUN 75

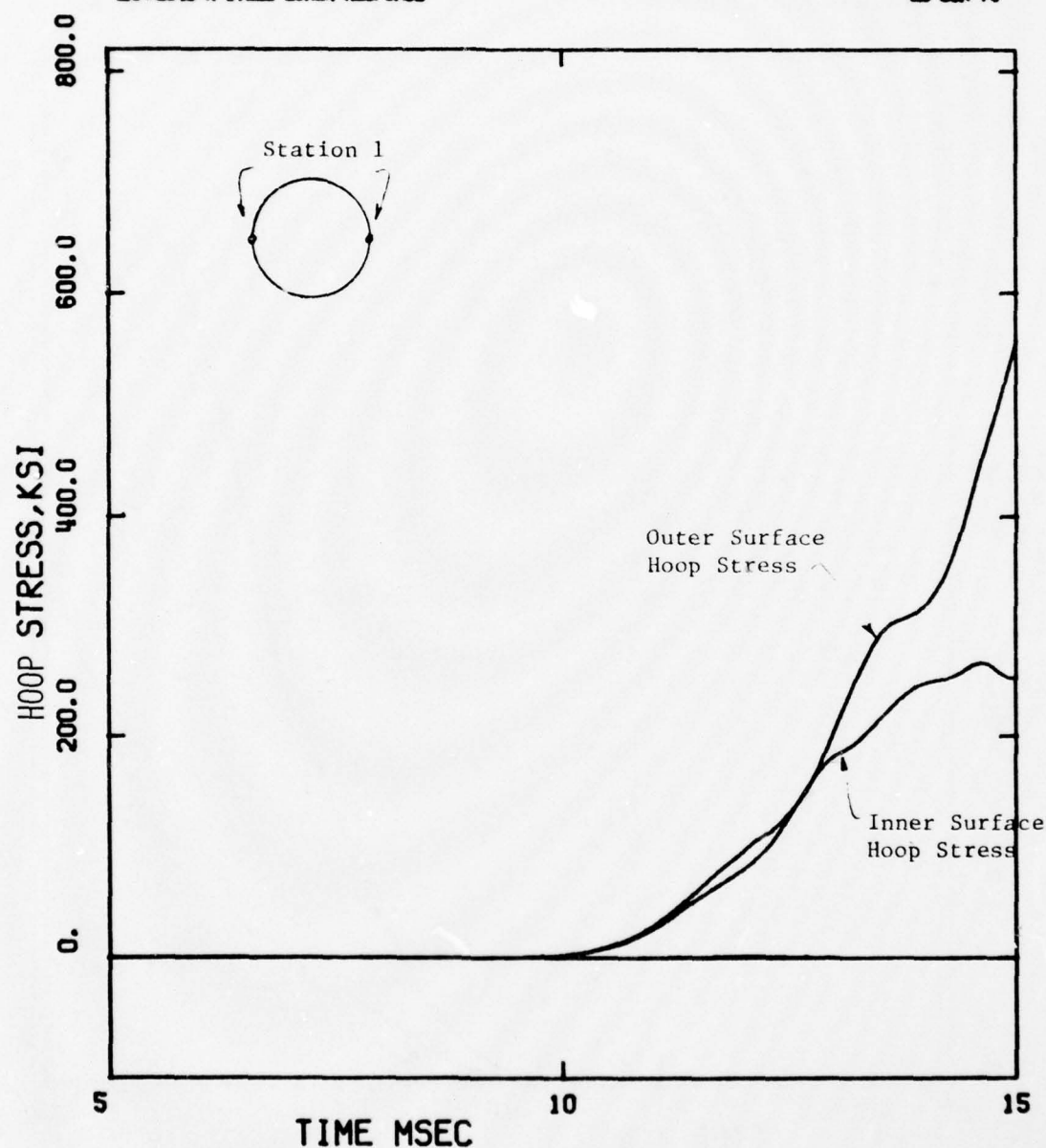


Figure 27. Compressive Hoop Stress History at Station 1 in 2" Steel Liner. Case M - Steel Liner in Tuff



CALIFORNIA RESEARCH AND TECHNOLOGY, INC.

LAP-2040-H STEEL LINER RESPONSE

23 JUN 75

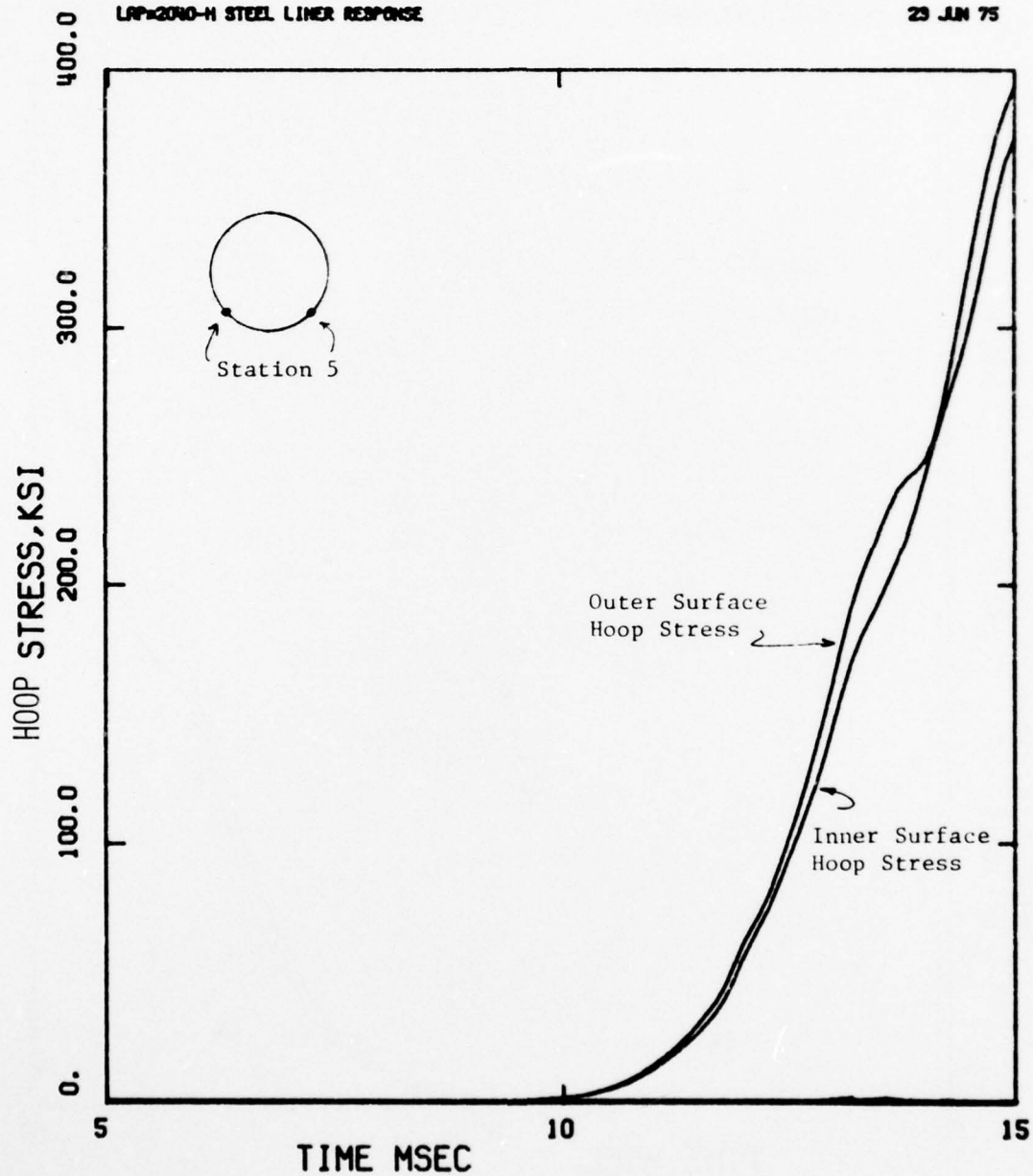


Figure 28. Compressive Hoop Stress History at Station 5 in 2" Steel Liner. Case M - Steel Liner in Tuff

CALIFORNIA RESEARCH AND TECHNOLOGY, INC.

LAP-20ND-H STEEL LINER RESPONSE

23 JUN 75

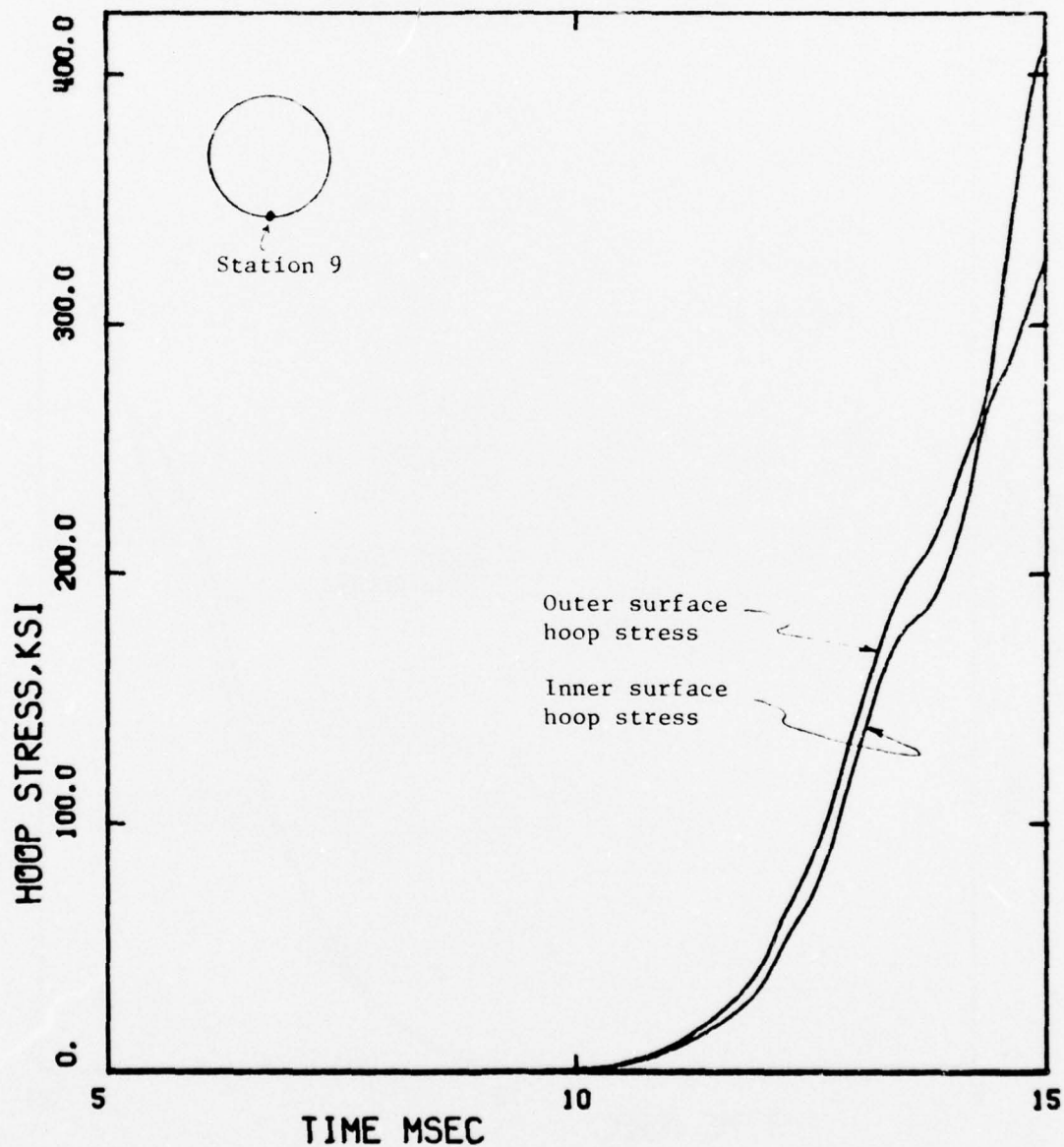


Figure 29. Compressive Hoop Stress History at Station 9 in 2" Steel Liner. Case M - Steel Liner in Tuff

CALIFORNIA RESEARCH AND TECHNOLOGY, INC.

LAP-2040-H STEEL LINER RESPONSE

23 JAN 75

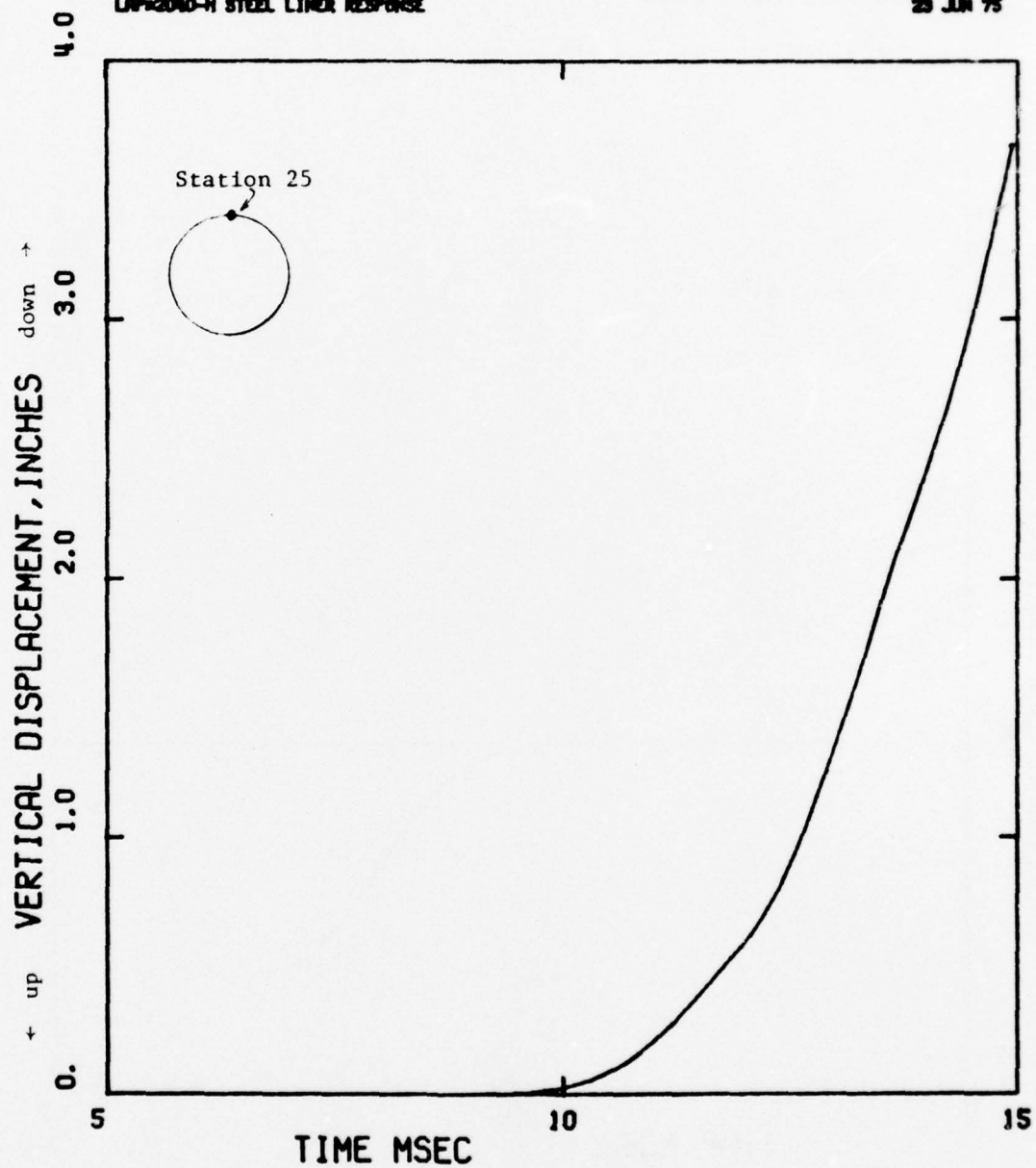


Figure 30. Vertical Displacement (Relative to Center of Mass of Steel Liner) of Station 25.  
Case M - 2" Steel Liner in Tuff

STA 9

CALIFORNIA RESEARCH AND TECHNOLOGY, INC.

LAP-2000-H STEEL LINER RESPONSE

23 JUN 75

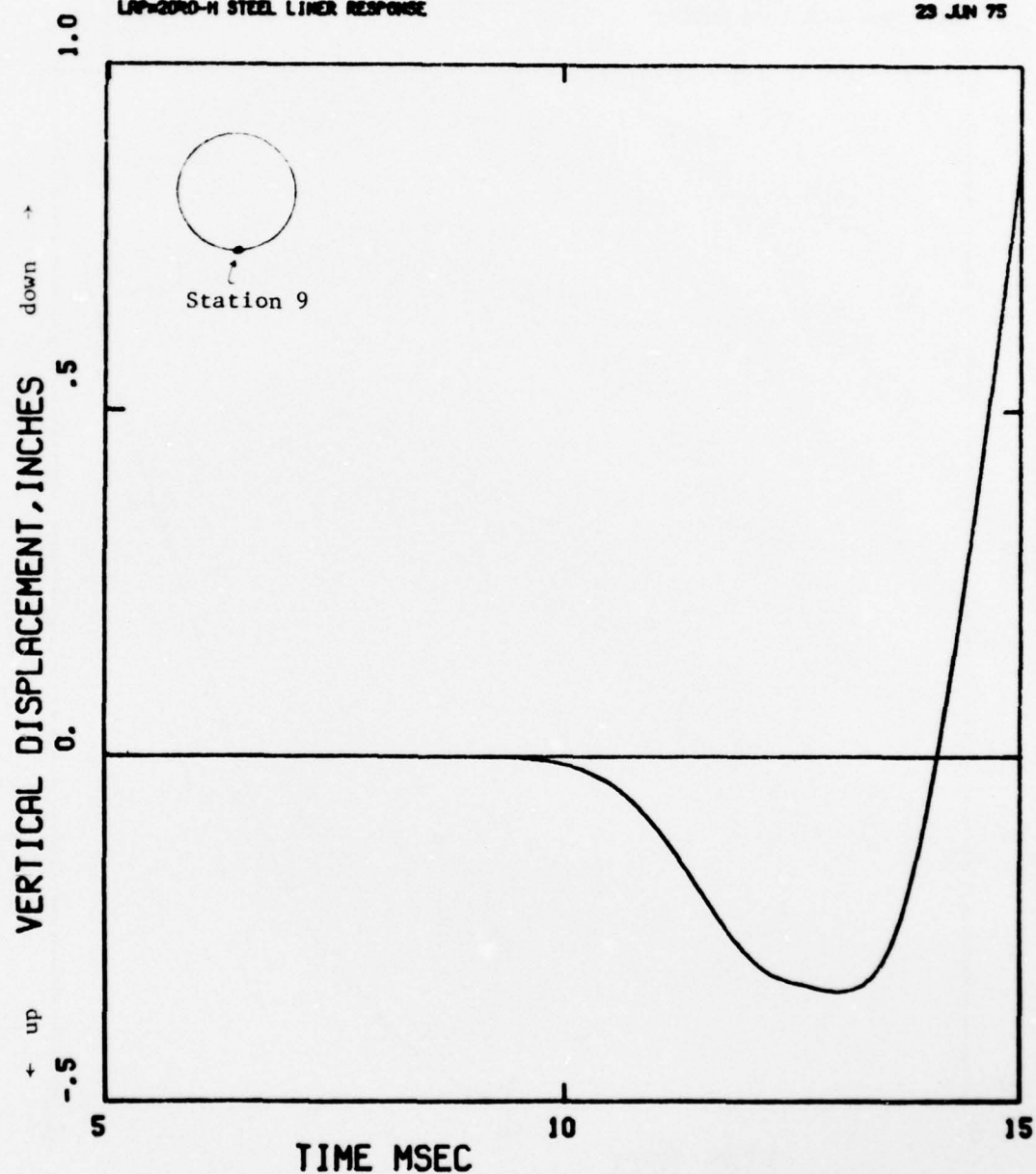


Figure 31. Vertical Displacement (Relative to Center of Mass of Steel Liner) of Station 9.  
Case M - 2" Steel Liner in Tuff



STA 1

CALIFORNIA RESEARCH AND TECHNOLOGY, INC.

LAP-2090-M STEEL LINER RESPONSE

29 JUN 75

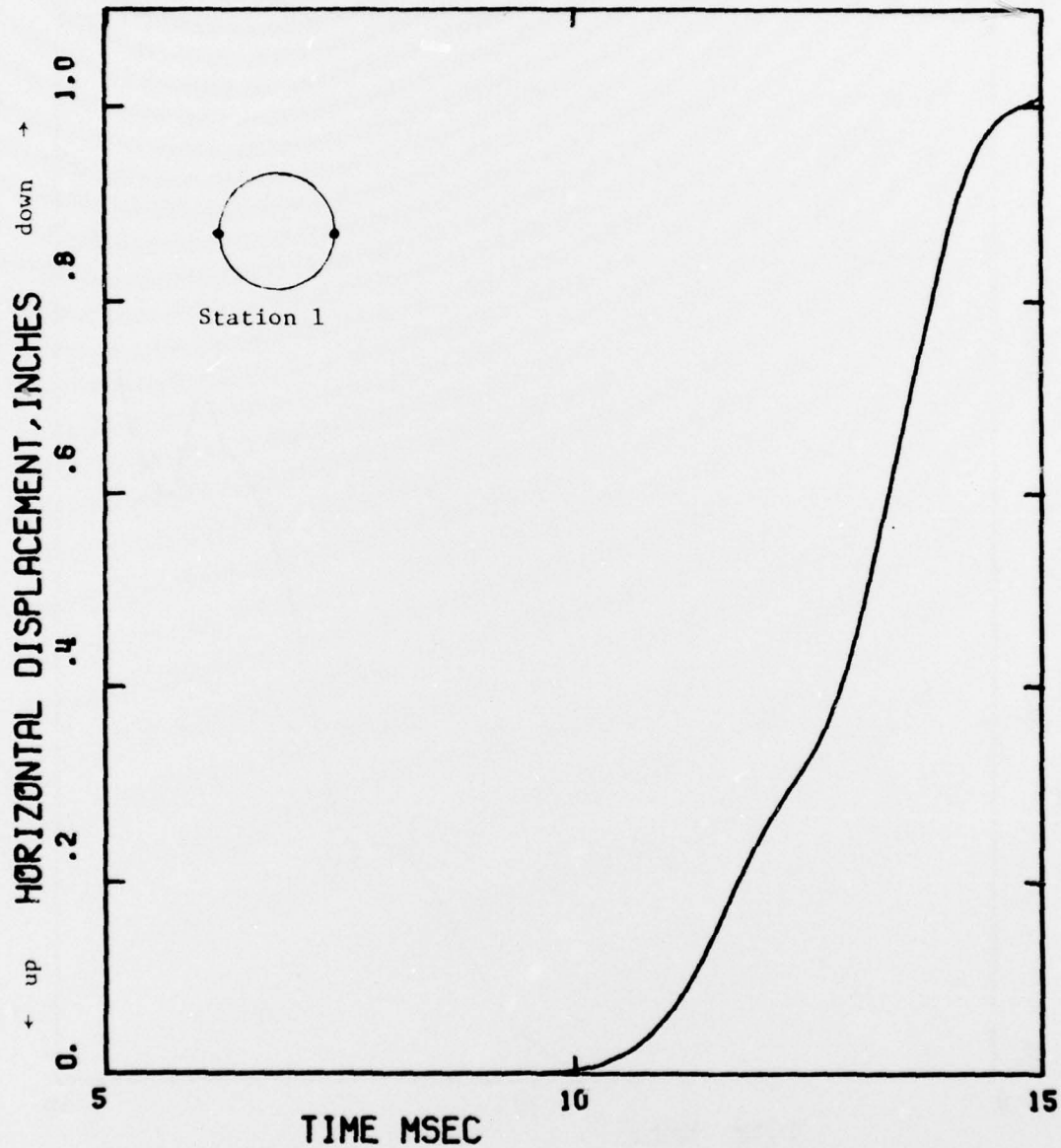


Figure 32. Horizontal (Radial) Displacement of Station 1 in 2" Steel Liner. Case M - Steel Liner in Tuff

STA 25

CALIFORNIA RESEARCH AND TECHNOLOGY, INC.

LAP-2000-M STEEL LINER RESPONSE

23 JUN 75

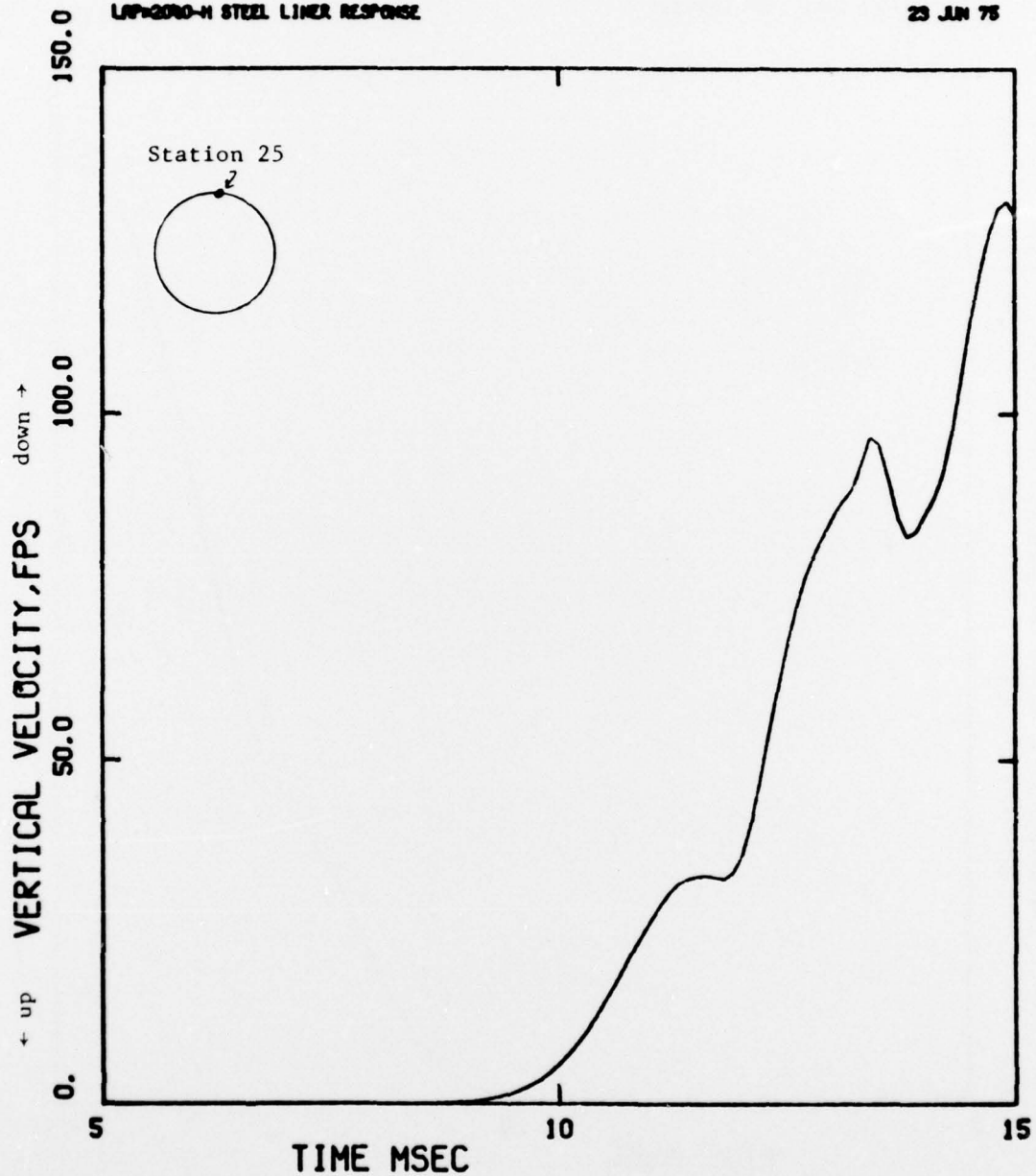


Figure 33. Vertical Velocity of Station 25 (Relative to Center of Mass of Steel Liner). Case M - 2" Steel Liner in Tuff

STA 1

CALIFORNIA RESEARCH AND TECHNOLOGY, INC.

LAP-2000-H STEEL LINER RESPONSE

23 JAN 75

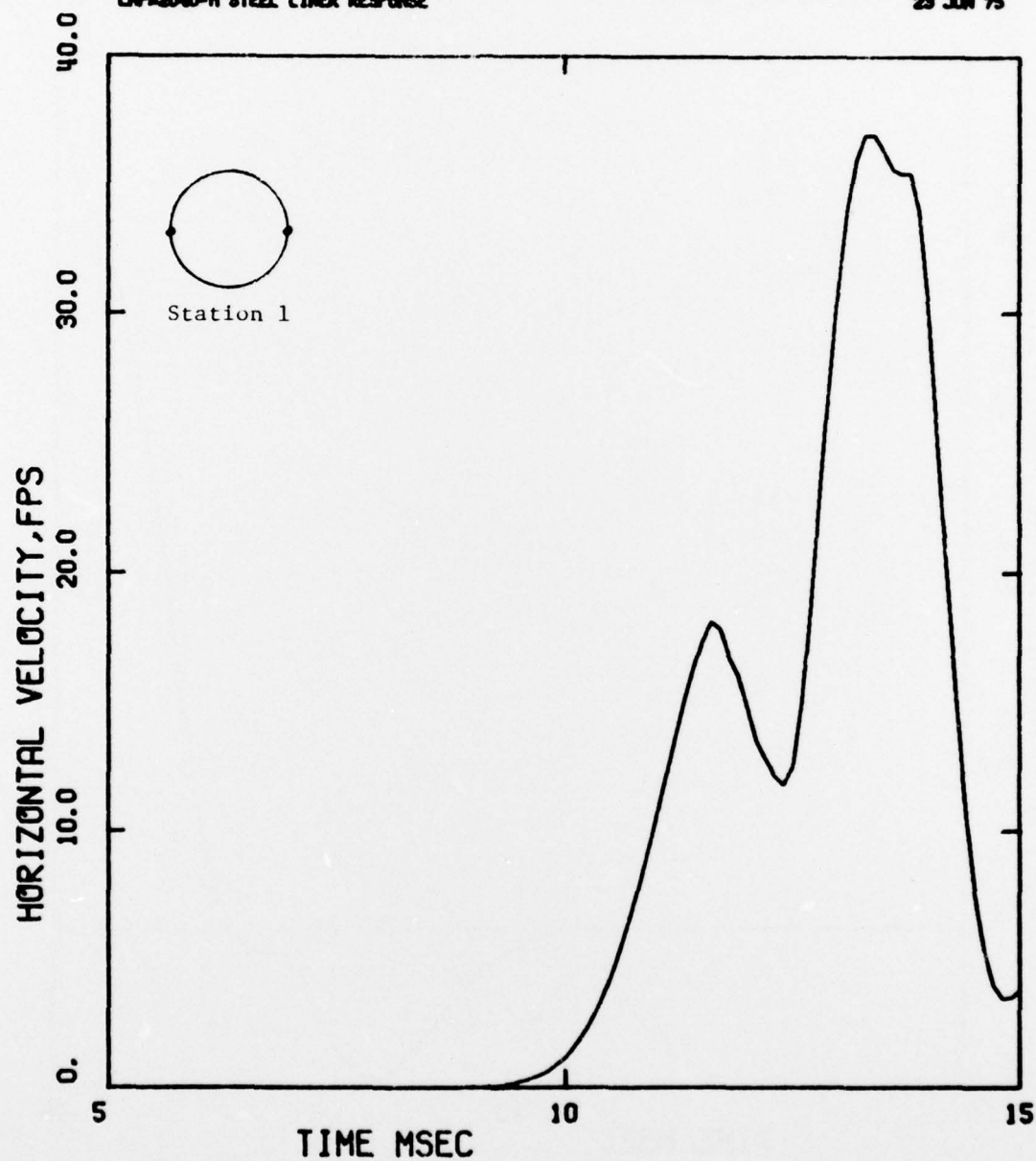


Figure 34. Horizontal (Radial) Velocity of Station 1  
in 2" Steel Liner. Case M - Steel Liner in Tuff

STA 9

CALIFORNIA RESEARCH AND TECHNOLOGY, INC.

LAP-2000-H STEEL LINER RESPONSE

23 JAN 75

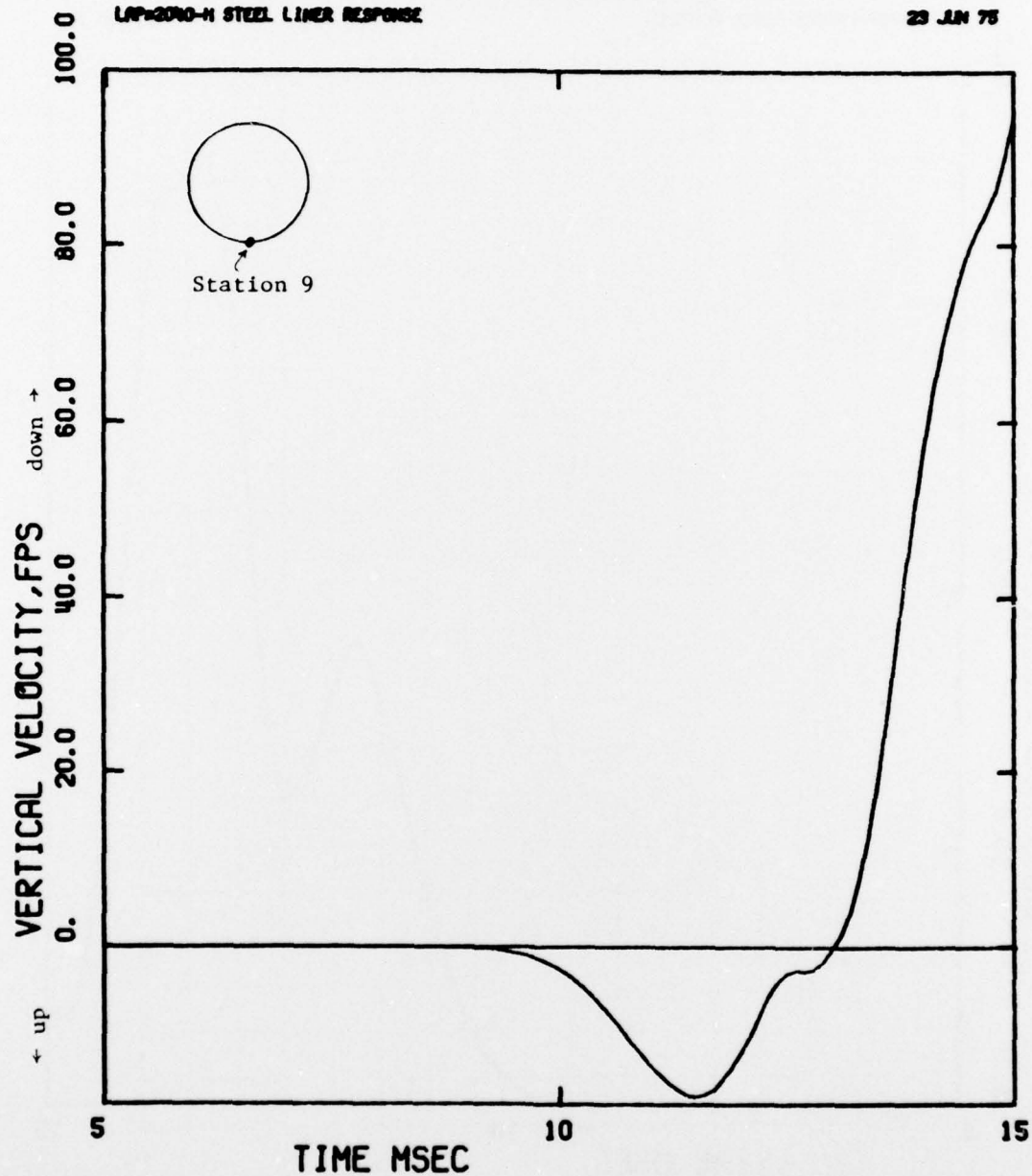


Figure 35. Vertical Velocity of Station 9 (Relative to Center of Mass of Steel Liner). Case M - 2" Steel Liner in Tuff



23 JUN 75 CALIFORNIA RESEARCH AND TECHNOLOGY  
LAP2000-1H S/C LINED TUNNEL IN TUFF WITH SC  
CYCLE 150

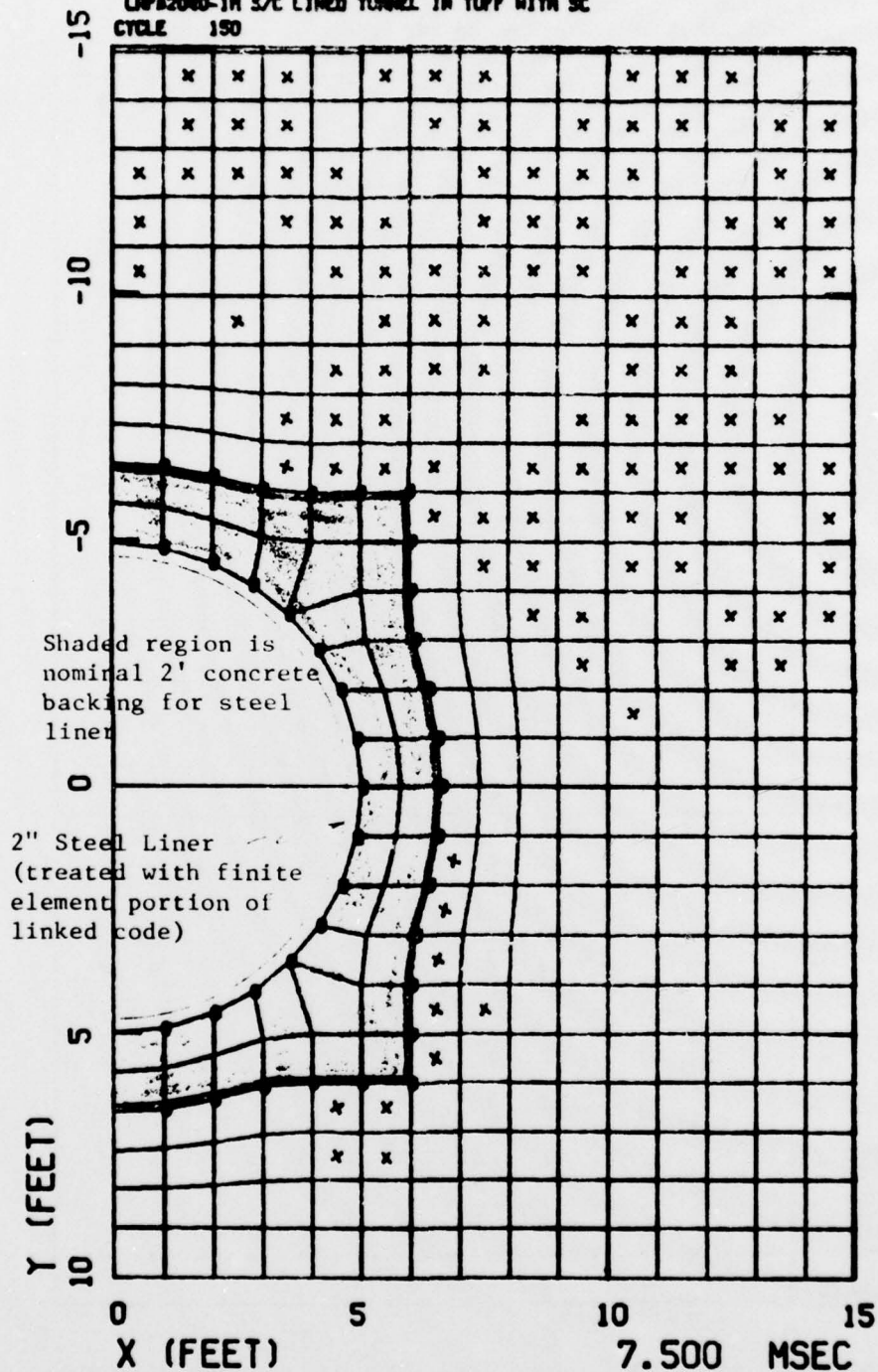


Figure 36. Computational Grid for Lagrangian Finite Difference Portion of LAP Code Solution for Case N - 2" Steel Liner with 2' Concrete Backing in Tuff with Explicit Shear Crack Failure Model ( $t = 7.5$  msec)

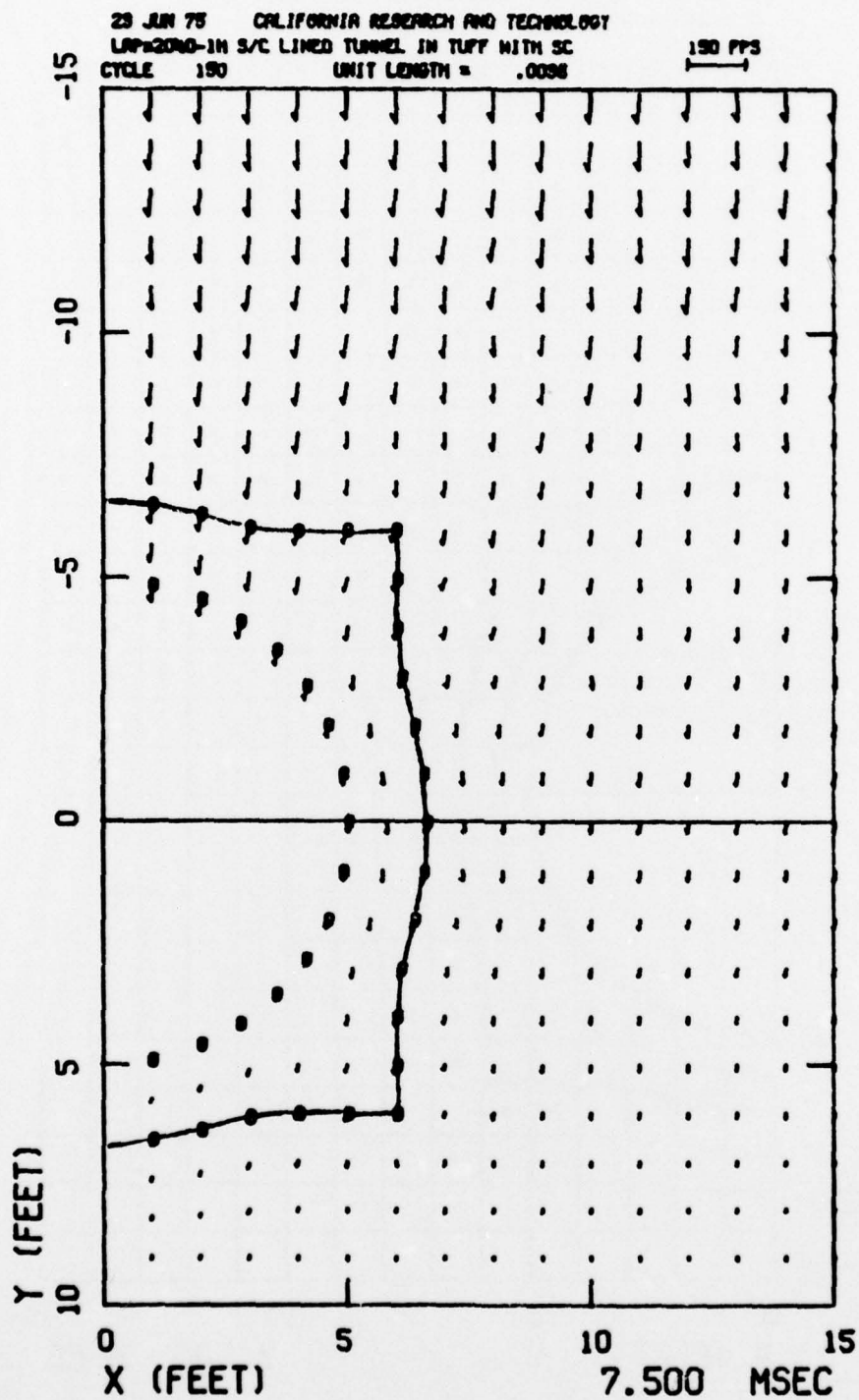


Figure 37. Velocity Field for Lagrangian Finite Difference Portion of LAP Code Solution for Case N - 2" Steel Liner with 2' Concrete Backing in Tuff with Explicit Shear Crack Failure Model (t = 7.5 msec)

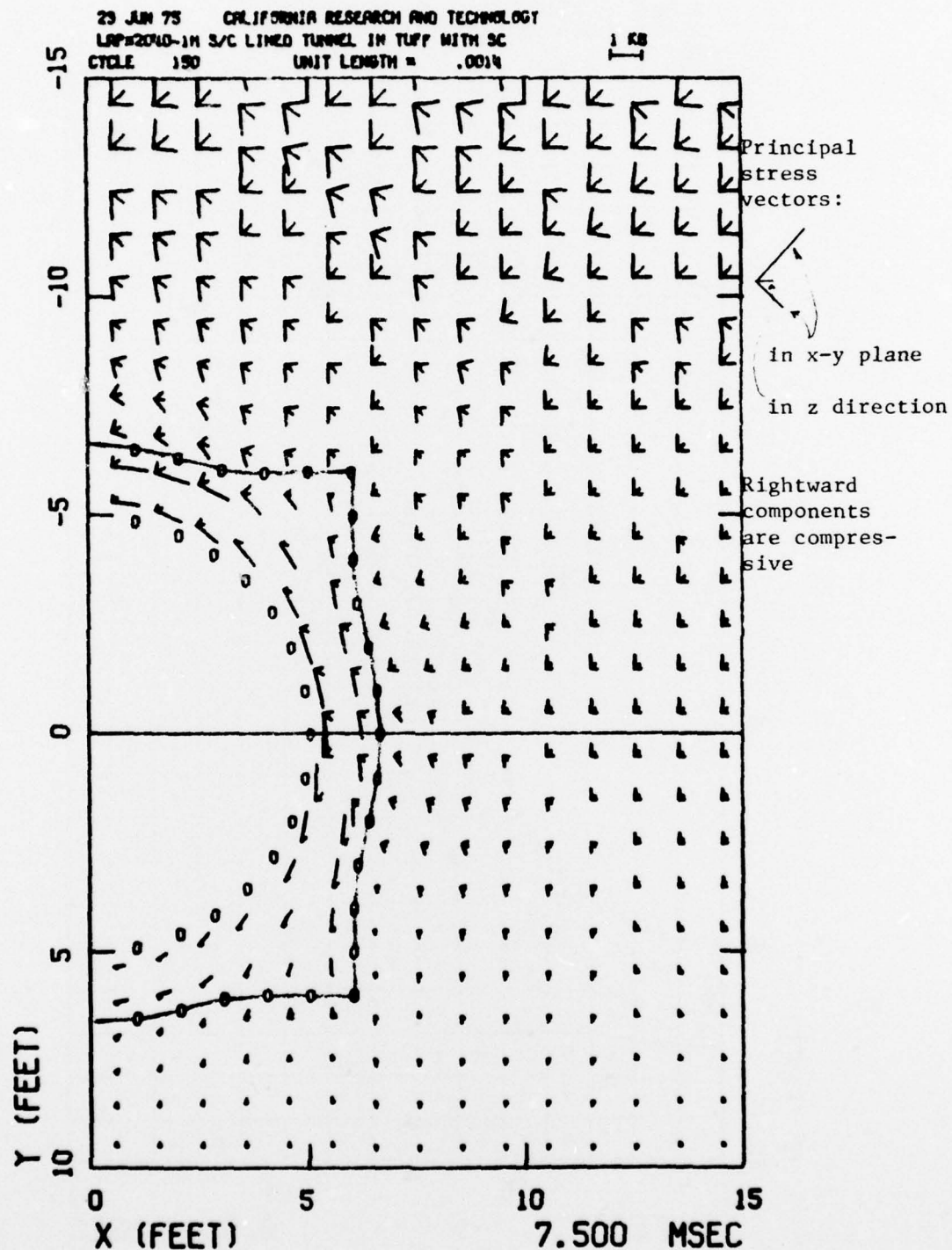


Figure 38. Principal Stress Field for Lagrangian Finite Difference Portion of LAP Code Solution for Case M - 2" Steel Liner in Tuff with Explicit Shear Crack Failure Model. (t = 7.5 msec)

22 JUN 75 CALIFORNIA RESEARCH AND TECHNOLOGY  
 LAP-2040-1H S/C LINED TUNNEL IN TUFF WITH SC  
 CYCLE 190

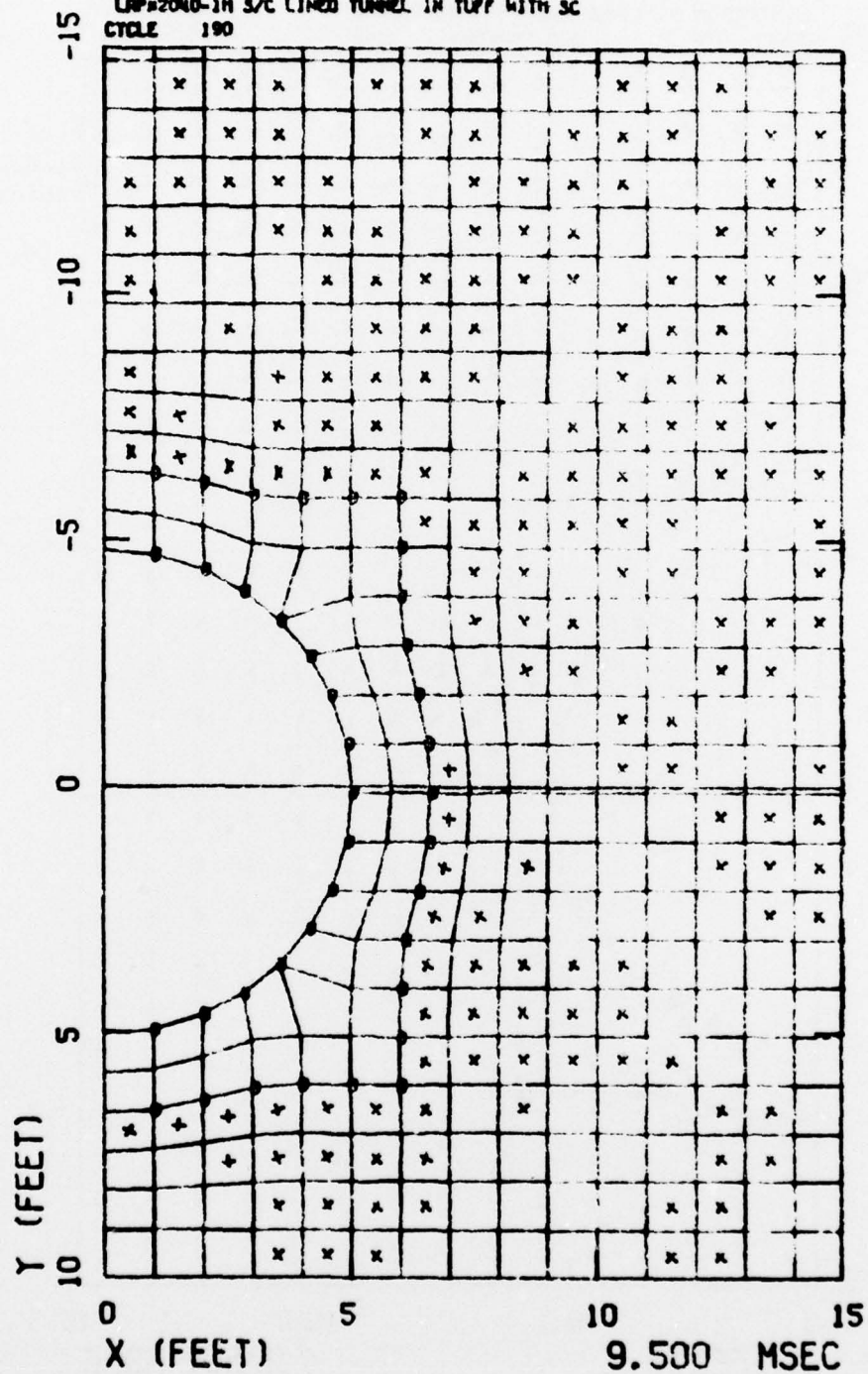


Figure 39. Computational Grid for Lagrangian Finite Difference Portion of LAP Code Solution for Case N - 2" Steel Liner with 2' Concrete Backing in Tuff with Explicit Shear Crack Failure Model ( $t = 9.5$  msec)



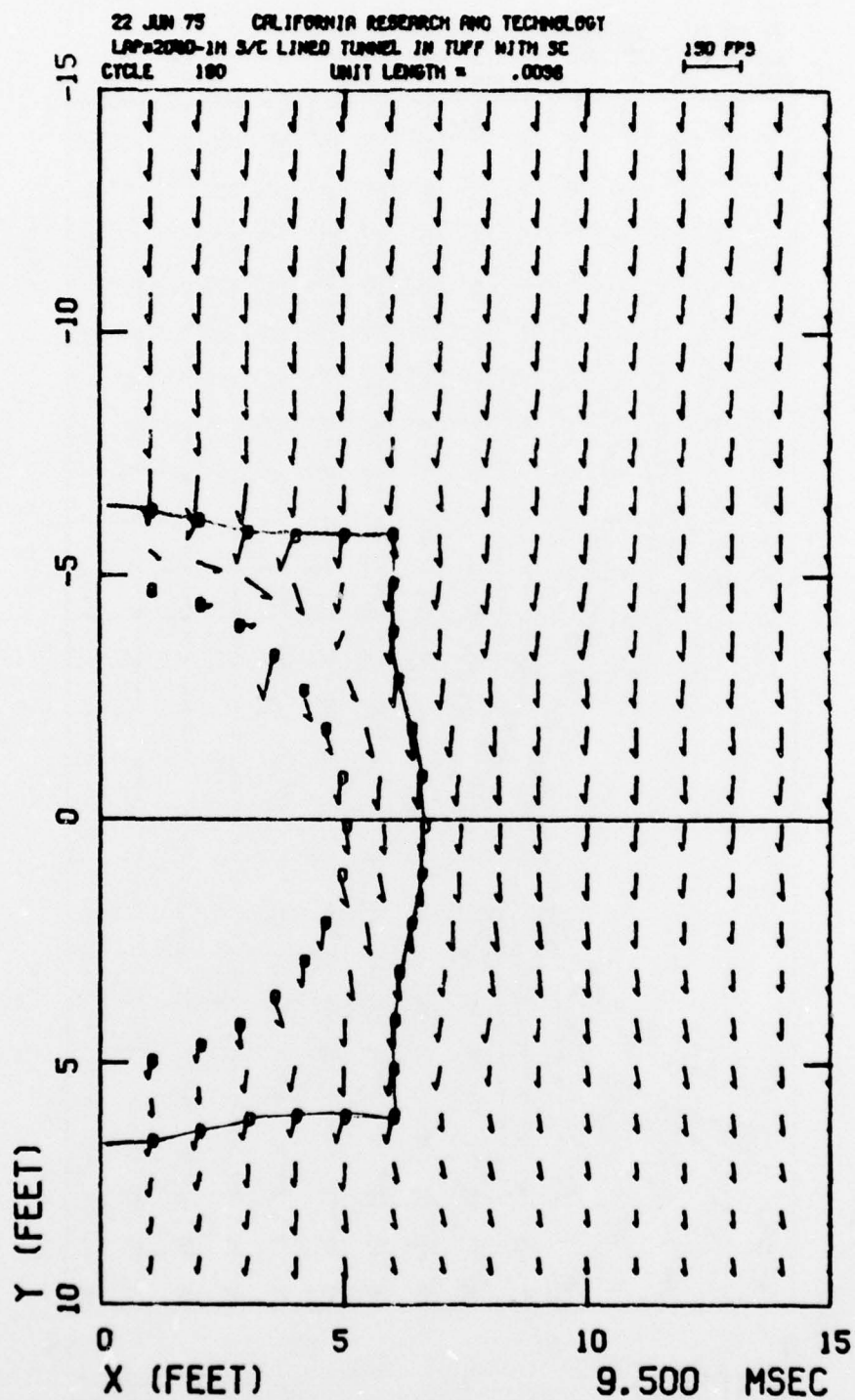


Figure 40. Velocity Field for Lagrangian Finite Difference Portion of LAP Code Solution for Case N - 2" Steel Liner with 2' Concrete Backing in Tuff with Explicit Shear Crack Failure Model. ( $t = 9.5$  msec)

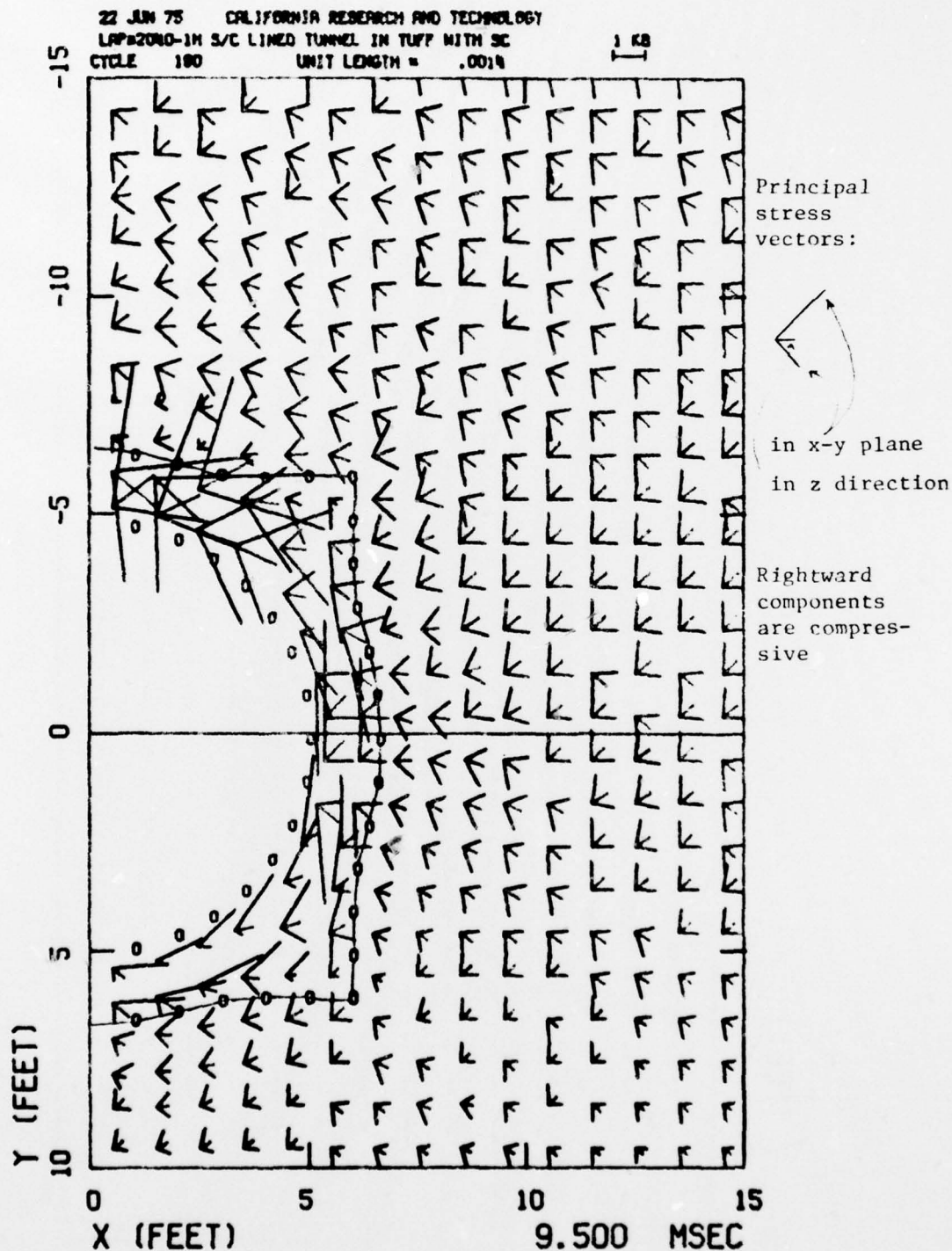


Figure 41. Principal Stress Field for Lagrangian Finite Difference Portion of LAP Code Solution for Case M - 2" Steel Liner in Tuff with Explicit Shear Crack Failure Model ( $t = 9.5$  msec)

## DISTRIBUTION LIST

### DEPARTMENT OF DEFENSE

Assistant to the Secretary of Defense  
Atomic Energy  
ATTN: Honorable Donald R. Cotter

Director  
Defense Advanced Rsch. Proj. Agency  
ATTN: NMRO  
ATTN: PMO  
ATTN: STO  
ATTN: Technical Library

Director  
Defense Civil Preparedness Agency  
Assistant Director for Research  
ATTN: Admin. Officer

Defense Communications Agency  
WWMCCS System Engineering Org.  
ATTN: Thomas Neighbors

Defense Documentation Center  
Cameron Station  
12 cy ATTN: TC

Director  
Defense Intelligence Agency  
ATTN: DB-4C, Edward O'Farrell  
ATTN: DI-7E

Director  
Defense Nuclear Agency  
ATTN: DDST  
ATTN: TISI, Archives  
2 cy ATTN: SPSS  
3 cy ATTN: TITL, Tech. Library

Chairman  
Dept. of Defense Explo. Safety Board  
ATTN: DD/S&SS

Commander  
Field Command  
Defense Nuclear Agency  
ATTN: FCPR  
ATTN: FCTMOF

Director  
Interservice Nuclear Weapons School  
ATTN: Document Control

Director  
Joint Strat. Tgt. Planning Staff, JCS  
ATTN: STINFO, Library

Chief  
Livermore Division Fld. Command, DNA  
Lawrence Livermore Laboratory  
ATTN: FCPL

Under Secretary of Def. for Rsch. & Engrg.  
ATTN: S&SS (OS)

### DEPARTMENT OF THE ARMY

Director  
BMD Advanced Tech. Ctr.  
Huntsville Office  
ATTN: CRDABH-S  
ATTN: ICRDABH-X

Dep. Chief of Staff for Rsch. Dev. & Acq.  
ATTN: Technical Library

Chief of Engineers  
ATTN: DAEN-MCE-D  
ATTN: DAEN-RDM

Deputy Chief of Staff for Ops. & Plans  
ATTN: Technical Library

Commander  
Harry Diamond Laboratories  
ATTN: DRXDO-TI, Tech. Library  
ATTN: DELHD-NP

Commander  
Redstone Scientific Information Ctr.  
U.S. Army Missile Command  
ATTN: Chief, Documents

Director  
U.S. Army Ballistic Research Labs.  
ATTN: DRDAR-BLE, W. Taylor  
ATTN: DRDAR-BLE, J. H. Keefer  
ATTN: DRXBR-X, Julius J. Meszaros  
ATTN: Tech. Library, Edward Baicy

Commander  
U.S. Army Engineer Center  
ATTN: ATSEN-SY-L

Division Engineer  
U.S. Army Engineer Div., Huntsville  
ATTN: HNDED-SR

Division Engineer  
U.S. Army Engineer Div., Ohio River  
ATTN: Technical Library

Director  
U.S. Army Engr. Waterways Exper. Sta.  
ATTN: Leo Ingram  
ATTN: John N. Strange  
ATTN: Technical Library  
ATTN: William Flathau  
ATTN: Guy Jackson

Commander  
U.S. Army Mat. & Mechanics Rsch. Ctr.  
ATTN: Technical Library

Commander  
U.S. Army Materiel Dev. & Readiness Cmd.  
ATTN: Technical Library

Commander  
U.S. Army Nuclear Agency  
ATTN: ATCA-NAW  
ATTN: Tech. Library

DEPARTMENT OF THE NAVY

Chief of Naval Material  
ATTN: MAT 0323

Chief of Naval Operations  
ATTN: OP 03EG  
ATTN: OP 981

Chief of Naval Research  
ATTN: Nicholas Perrone  
ATTN: Technical Library  
ATTN: Code 464, Jacob L. Warner  
ATTN: Code 464, Thomas P. Quinn

Officer-In-Charge  
Civil Engineering Laboratory  
Naval Construction Battalion Center  
ATTN: Stan Takahashi  
ATTN: R. J. O'Dello  
ATTN: Technical Library

Commander  
Naval Electronic Systems Command  
Naval Electronic Systems Cmd. Hqs.  
ATTN: PME, 117-21A

Commander  
Naval Facilities Engineering Command  
Headquarters  
ATTN: Code 03A  
ATTN: Code 04B  
ATTN: Technical Library

Superintendent (Code 1424)  
Naval Postgraduate School  
ATTN: Code 2124, Tech. Rpts. Librarian

Director  
Naval Research Laboratory  
ATTN: Code 2600, Tech. Library

Officer-In-Charge  
Naval Surface Weapons Center  
ATTN: Code WA501, Navy Nuc. Prgms. Off.

Commander  
Naval Surface Weapons Center  
Dahlgren Laboratory  
ATTN: Technical Library

Commanding Officer  
Naval Underwater Systems Center  
ATTN: Code EM, Jack Kalinowski

President  
Naval War College  
ATTN: Technical Library

Commanding Officer  
Naval Weapons Evaluation Facility  
ATTN: Technical Library

Director  
Strategic Systems Project Office  
ATTN: NSP-43, Tech. Library

DEPARTMENT OF THE AIR FORCE

AF Geophysics Laboratory, AFSC  
ATTN: LWL, K. C. Thompson  
ATTN: SUOL, Rsch. Library

AF Institute of Technology, AU  
ATTN: Library, AFIT Bldg. 640, Area B

AF Weapons Laboratory, AFSC  
ATTN: DEP, Jimmie L. Bratton  
ATTN: DES-S, M. A. Plamondon  
ATTN: SUL

Headquarters  
Air Force Systems Command  
ATTN: DLCAW

Commander  
Foreign Technology Division, AFSC  
ATTN: NICD, Library

HQ USAF/IN  
ATTN: INATA

HQ USAF/PR  
ATTN: PRE

HQ USAF/RD  
ATTN: RDQSM

Commander  
Rome Air Development Center, AFSC  
ATTN: EMTLD, Doc. Library

SAMSO/MN  
ATTN: MNN

Commander In Chief  
Strategic Air Command  
ATTN: NRI-STINFO, Library

DEPARTMENT OF ENERGY

Department of Energy  
Albuquerque Operations Office  
ATTN: Doc. Control for Tech. Library

Department of Energy  
Division of Headquarters Services  
Library Branch, G-043  
ATTN: Doc. Control for Class. Tech. Lib.

Department of Energy  
Nevada Operations Office  
ATTN: Doc. Control for Tech. Library

University of California  
Lawrence Livermore Laboratory  
ATTN: Tech. Info. Dept., L-3  
ATTN: Larry W. Woodruff, L-96

Los Alamos Scientific Laboratory  
ATTN: Doc. Control for Reports Library  
ATTN: Doc. Control for R. J. Bridwell

Sandia Laboratories  
Livermore Laboratory  
ATTN: Doc. Control for Tech. Library



DEPARTMENT OF ENERGY (Continued)

Sandia Laboratories  
ATTN: L. Hill  
ATTN: Doc. Control for 3141, Sandia Rpt. Coll.

Union Carbide Corporation  
Holifield National Laboratory  
ATTN: Doc. Control for Tech. Library  
ATTN: Civil Def. Res. Proj.

OTHER GOVERNMENT AGENCY

Department of the Interior  
Bureau of Mines  
ATTN: Tech. Library

DEPARTMENT OF DEFENSE CONTRACTORS

Aerospace Corporation  
ATTN: Tech. Info. Services

Agabian Associates  
ATTN: M. Agabian

Applied Theory, Inc.  
2 cy ATTN: John G. Trulio

Avco Research & Systems Group  
ATTN: Research Library A830, Rm. 7201

Battelle Memorial Institute  
ATTN: Technical Library

The BDM Corporation  
ATTN: Technical Library

The Boeing Company  
ATTN: Aerospace Library

California Research & Technology, Inc.  
ATTN: Sheldon Shuster  
ATTN: Technical Library  
ATTN: Ken Kreyenhagen  
ATTN: M. Rosenblatt  
ATTN: J. E. Eggum  
ATTN: Y. M. Ito

Calspan Corporation  
ATTN: Technical Library

Civil/Nuclear Systems Corp.  
ATTN: Robert Crawford

University of Dayton  
Industrial Security Super., KL-505  
ATTN: Hallock F. Swift

University of Denver  
Colorado Seminary  
Denver Research Institute  
ATTN: Sec. Officer for J. Wisotski

EG&G, Inc.  
Albuquerque Division  
ATTN: Technical Library

Gard, Incorporated  
ATTN: G. L. Neidhardt

DEPARTMENT OF DEFENSE CONTRACTORS (Continued)

General Electric Company  
TEMPO-Center for Advanced Studies  
ATTN: DASAC

IIT Research Institute  
ATTN: Milton R. Johnson  
ATTN: R. E. Welch  
ATTN: Technical Library

Institute for Defense Analyses  
ATTN: IDA Librarian, Ruth S. Smith

Kaman Avidyne  
Division of Kaman Sciences Corp.  
ATTN: Technical Library  
ATTN: Norman P. Hobbs  
ATTN: E. S. Criscione

Kaman Sciences Corporation  
ATTN: Library

Lockheed Missiles and Space Co., Inc.  
ATTN: Tech. Info. Ctr., D/Coll.  
ATTN: Tom Geers, D/52-33, Bldg. 205

Lovelace Foundation for Medical Education & Rsch.  
ATTN: Asst. Dir. of Res., Robert K. Jones  
ATTN: Technical Library

McDonnell Douglas Corporation  
ATTN: Robert W. Halprin

Merritt CASES, Incorporated  
ATTN: J. L. Merritt  
ATTN: Technical Library

Nathan M. Newmark Consulting Engineering Services  
University of Illinois  
ATTN: Nathan M. Newmark

Physics International Company  
ATTN: Doc. Control for Dennis Orphal  
ATTN: Doc. Control for Fred M. Sauer  
ATTN: Doc. Control for Larry A. Behrmann  
ATTN: Doc. Control for Robert Swift  
ATTN: Doc. Control for E. T. Moore  
ATTN: Doc. Control for Tech. Library

R & D Associates  
ATTN: Robert Port  
ATTN: William B. Wright, Jr.  
ATTN: Albert L. Latter  
ATTN: Henry Cooper  
ATTN: Technical Library  
ATTN: Jerry Carpenter  
ATTN: J. G. Lewis  
ATTN: Harold L. Brode

Science Applications, Inc.  
ATTN: David Bernstein  
ATTN: D. E. Maxwell

Science Applications, Inc.  
ATTN: Technical Library

Southwest Research Institute  
ATTN: Wilfred E. Baker  
ATTN: A. B. Wenzel

DEPARTMENT OF DEFENSE CONTRACTORS (Continued)

SRI International  
ATTN: George R. Abrahamson  
ATTN: Burt R. Gasten

Systems, Science and Software, Inc.  
ATTN: Ted Cherry  
ATTN: Technical Library  
ATTN: Thomas D. Riney  
ATTN: Donald R. Grine

Terra Tek, Inc.  
ATTN: Technical Library  
ATTN: Sidney Green

Tetra Tech., Inc.  
ATTN: Li-San Hwang  
ATTN: Technical Library

TRW Defense & Space Sys. Group  
ATTN: Pravin Bhutta, R1-1104  
2 cy ATTN: Peter K. Dai, R1/2170  
ATTN: Tech. Info. Center/S-1930

DEPARTMENT OF DEFENSE CONTRACTORS (Continued)

TRW Defense & Space Sys. Group  
San Bernardino Operations  
ATTN: E. Y. Wong, 527/712

Universal Analytics, Inc.  
ATTN: E. I. Field

The Eric H. Wang Civil Engineering Rsch. Fac.  
University Station  
The University of New Mexico  
ATTN: Neal Baum  
ATTN: Larry Bickle

Weidlinger Assoc. Consulting Engineers  
ATTN: Melvin L. Baron

Weidlinger Assoc. Consulting Engineers  
ATTN: J. Isenberg

Westinghouse Electric Corp.  
Marine Division  
ATTN: W. A. Volz